1992A&AS...92..481B

ASTRONOMY & ASTROPHYSICS
SUPPLEMENT SERIES

Astron. Astrophys. Suppl. Ser. **92,** 481-516 (1992)

A magnitude-limited spectroscopic and photometric survey of ρ Ophiuchus X-ray sources*

J. Bouvier[1] and I. Appenzeller[2]

[1] Observatoire de Grenoble, Groupe d'Astrophysique, CERMO B.P. 68, F-38402 Saint-Martin-d'Hères Cedex
[2] Landessternwarte Königstuhl 6900 Heidelberg, Germany

Received April 9; accepted June 17, 1991

Abstract. — We report results from a spectroscopic and photometric survey of optical counterpart candidates of X-ray sources in the ρ Ophiuchus dark cloud. Low and medium resolution spectrograms are presented for 47 stars lying in 29 *Einstein* IPC X-ray error circles. Hα is seen in emission above the continuum in the spectra of 27 stars, 12 of which were not detected during previous Hα surveys of the cloud. The Hα equivalent width is less than 10 Å in most of the stars. The emission-line stars also have strong Li I λ6707 absorption indicative of stellar youth, which indicates that they are pre-main sequence cloud members. Three additional stars without Hα emission are most certainly cloud members. In total, 30 pre-main sequence stars are identified as being likely optical counterparts of 24 X-ray sources. An HR diagram constructed for these stars using spectral types and stellar luminosities derived in this study shows that they have an age between 10^6 to 10^7 yr, and a mass in the range from 0.3 to 2.5 $M_\odot$. We conclude that the optical counterparts of the ρ Ophiuchus X-ray sources mostly are weak emission-line T Tauri stars with an evolutionary status similar to that of *bona fide* T Tauri stars found in other stellar formation regions.

Key words: interstellar medium: clouds: individual: Barnard 42, stars: pre-main-sequence, X-rays: sources, stars: binaries: visual, stars: circumstellar matter.

1. Introduction.

At a distance of 170 pc, the ρ Ophiuchus dark cloud (Barnard 42) is one of the nearest site of star formation. It is part of a vast molecular complex which extends over more than 25^2 degrees on the sky and whose total mass is of the order of 10^4 $M_\odot$ (de Geus *et al.* 1990). Large-scale mapping of the ^{13}CO and C^{18}O molecular gas distribution shows that the ρ Ophiuchus dark cloud consists of two major clumps of gas with associated "streamers" extending more than 10 pc away in the North-East direction (Wilking & Lada 1983, Loren 1989). The gas distribution, as well as the increased density of young stellar objects at the southwestern edge of the dark cloud, led Vrba (1977) to suggest that a compression front originating from the nearby Sco OB2 association propagates through the cloud in the northeastward direction, trigerring star formation. Vrba's shock hypothesis was later confirmed by Loren & Wootten (1986) who found steep molecular density gradients at the southwestern edge of the cloud facing the Sco OB2 association.

Multi-wavelength surveys of the dark cloud reveal that it is an active site of star formation, with an unusually high star formation efficiency ($SFE \geq 22\%$, Wilking *et al.* 1989) compared to other dark clouds such as Taurus-Auriga. Early optical surveys list 75 emission-line stars (Haro 1949, Struve & Rudkjøbing 1949, Dolidze & Arakelyan 1959), while more recent Hα surveys with greater sensitivity have increased this number to more than 110 (Wilking *et al.* 1987). Most of these optically visible stars are located at the edge of the densest parts of the cloud, where the extinction is the lowest. Only 25 or so, however, have been studied at low spectral resolution and are listed in Herbig & Bell's (1988) catalogue of emission-line objects. Near- and far-infrared surveys of the central, densest regions of the cloud, where the visual extinction may reach up to 100 magnitudes, have led to the discovery of as many as 78 IR sources, some of which have no optical counterparts and form a deeply embedded, possibly bound, protostellar cluster (see Wilking *et al.* 1989 and references therein). In the same region, a deep VLA survey at 5 GHz revealed a cluster of 14 faint radio sources (Leous *et al.* 1990), some of which are associated with near-IR sources. On a larger scale, medium-sensitivity surveys at 1.4 and 5 GHz led to the detection of 12 additional stellar

* Based on observations collected at the European Southern Observatory, La Silla, Chile

© European Southern Observatory • Provided by the NASA Astrophysics Data System

1992A&AS...92..481B

radio sources (André *et al.* 1987, Stine *et al.* 1988), which sometimes exhibit extreme flarelike variability indicative of non-thermal emission processes (André 1987). Finally, radio continuum observations at 1.3 mm led to positive detections in 16 of the 20 young stellar objects observed, which suggests that most of them are surrounded by cold circumstellar material (André *et al.* 1990).

The present study is directly connected with the X-ray survey of the cloud conducted by Montmerle *et al.* (1983, hereafter MKFG) with the *Einstein* Observatory. From repeated observations of various parts of the cloud, they confidently detected 47 X-ray sources and listed 20 additional source candidates near the detection limit. Thirty ρ Ophiuchus X-ray (ROX) sources had possible counterparts at other wavelengths, which led MKFG to suggest that most ROX sources are pre-main sequence cloud members. This suggestion was further supported by the large flux variations most sources exhibit at X-ray wavelengths and by their spatial distribution at the periphery of the densest regions of the cloud in areas where the gas column density is too low to significantly absorb X-ray emission. Assuming that the sources are cloud members, MKFG derived X-ray luminosities between 10^{30} and a few 10^{31} erg. s^{-1}, quite typical of X-ray luminosities measured for T Tauri stars in other stellar formation regions (e.g., Walter *et al.* 1989, Feigelson & Kriss 1989, Strom *et al.* 1990).

In order to assess the evolutionary status of the ROX sources, we undertook a spectroscopic and photometric survey of 47 stars located in 29 X-ray error circles. Low- and medium-resolution spectrograms covering the 3700-7500 Å range, as well as visual and some near-IR photometry, obtained for these objects are presented in Section 2. Spectral types, Hα, Hβ, and Ca II H-K equivalent widths, as well as stellar luminosities and visual extinctions are derived in Section 3. We find that 3 stars have a spectral type which strongly varies with wavelength, being earlier at shorter wavelengths. The origin of these composite spectra is discussed. The probability that the observed stars are cloud members is investigated in Section 4 on the basis of their spectroscopic and photometric properties. We identify 30 pre-main sequence cloud members as being likely optical counterparts of 24 ROX sources, while most of the 17 remaining stars are probably background giants. An HR diagram is constructed for the X-ray emitting pre-main sequence stars to derive their evolutionary status and physical properties. Finally, the properties of optical pairs of emission-line stars lying in the same X-ray error circle are discussed. The results are summarized in Section 5.

2. Observations.

We studied 47 optically visible stars lying in the *Einstein* IPC error circles of 29 ROX sources. Eighteen additional sources detected by MKFG were not included in this study for the following reasons: 6 of them (ROX 17, 22, 23, 24, 26, 46) have no visible stellar counterparts on POSS red prints, while the optical counterparts of 9 other (ROX 11, 15, 18, 19, 25, 27, 28, 32, 41) were too faint to be observed. The optical counterparts of ROX 1 (= Struve & Rudkjøbing (1949) object # 2, a non-emission-line star) and ROX 37 (= SAO 184429) are bright, presumably field stars, and were not considered. Finally, no stars could be seen near the ROX 13 error circle on a blue-sensitive TV monitor during the observations. The five stellar-like spots seen on POSS red prints at that position are artifacts.

Low- and medium-resolution spectrograms, as well as visual and near-IR photometry, were obtained at ESO La Silla, Chile, between June 1983 and May 1986. Coordinates of the 47 stars in our sample are listed in Table 1 and finding charts are provided in Figure 1. The coordinates were measured on POSS red prints with an accuracy of $\pm$ 2 arcsec using the $X-Y$ measuring machine of the Institut d'Astrophysique de Paris. In order to avoid semantic confusion between the X-ray sources and their optical counterpart candidates, the latter were given the name "ROXs # n" (which stands for ROXstar # n), where # n is the X-ray source number. Thus, ROX 2 refers to the X-ray source detected by MKFG, while ROXs 2 refers to the star observed in the corresponding X-ray error circle. The distinction is made necessary by the fact that we have no *a priori* knowledge of which star in the error circle is the actual optical counterpart of the X-ray source. When several stars were observed in a given error circle, the star's name is followed by an arabic letter (e.g., ROXs 20A, 20B) with the alphabetic order corresponding to increasing right ascension. A cross-identification list is given in Table 2 for stars which have been detected in previous surveys of the cloud.

2.1. Spectroscopy.

Spectroscopic observations were conducted at ESO La Silla during seven observing periods between July 1983 and May 1986. The Journal of Observations is given in Table 3. Low-and medium-resolution spectrograms were obtained at the ESO 1.5 m telescope using the Boller & Chivens spectrograph. The detector was either the Image Dissector Scanner (IDS) or photographic plates coupled to an EMI image tube. During five observing periods, the spectroscopic study of the ROX optical counterparts was merely a backup program and the instrumental set-up was dictated by the primary scientific program. Therefore, the spectrograms presented here do not constitute an homogeneous data set but spectral dispersion ranges from 39 to 224 Å/mm. Nevertheless, the spectral range from 3700 Å to 7500 Å was covered for most of the stars.

Low-resolution spectrograms were obtained with a dispersion of 114, 116, 172, and 224 Å/mm using the IDS

© European Southern Observatory • Provided by the NASA Astrophysics Data System

1992A&AS...92..481B

detector, which leads to a spectral resolution of 5 to 10 Å. The star and the sky 1 arcmin apart were simultaneously recorded through 4*4 arcsec^2 apertures. Each stellar exposure was followed by a 10 s integration on a He-Ar lamp for subsequent wavelength calibration. At the beginning and at the end of each night, a 30 mn flat-field exposure was obtained on the telescope dome illuminated with a white lamp. The flat-field exposures were later used to correct the pixel-to-pixel variations of the detector response while spectrophotometric standards were observed each night in the same conditions than the program stars in order to derive the low-frequency response curve of the instrument. When the observations were obtained under photometric conditions, the spectrograms were flux calibrated using the spectrophotometric standards observed on the same night. Spectrograms were corrected for atmospheric extinction assuming mean extinction coefficients for La Silla. Finally, spectroscopic standards with spectral types in the range from G4 to M5 were selected from Gliese's (1969) catalogue and observed under the same conditions. They were later used as templates for the spectral classification of the program stars.

For some of the brightest stars, medium-resolution spectrograms were obtained with a dispersion of 39 Å/mm in the blue spectral region (3700-5000 Å) and 59.5 Å/mm in the red region (5800-7700 Å) using a 3-stage EMI image tube and photographic plates. The spectrogram was recorded through a 2 × 30 arcsec slit and a rocking plate was used to increase the height of the spectrogram to 560 microns on the photographic plate. After each stellar exposure, an He-Ar spectrum was obtained for wavelength calibration purposes and spectrophotometric standards were observed to derive the instrumental response. In addition, flux calibration plates were obtained using the ESO spot sensitometer in order to convert photographic densities to relative intensities. The plates were digitalized at ESO Garching using the PDS 1010A microdensitometer with a 10 × 10 microns aperture. The resulting spectral resolution is 2 and 3 Å in the blue and red spectral regions, respectively. The digitalized spectrograms were reduced at ESO Garching using the standard IHAP reduction package. No sky subtraction nor photometric calibration were attempted. Consequently, spectrograms obtained with the EMI tube are affected by sky emission lines.

2.2. PHOTOMETRY.

Optical photometry was conducted in the Johnson *UBV*, Cousins *UBVRI*, and Geneva 7-color systems at ESO La Silla between June 1983 and June 1984 with the ESO 50 cm, ESO 1 m, Bochum 60 cm, and Swiss 70 cm telescopes. The instrumentation used at the ESO 50 cm, ESO 1 m, and Swiss 70 cm telescopes as well as the observational procedure and the reduction process are described in Bouvier *et al.* (1988) and will not be repeated here. Extensive photometric data for 8 ROX optical counterparts (ROXs 3, 6, 8, 21, 29, 34, 44, and 47A) appear in that paper. Johnson *UBV* photometry was done at the Bochum 60 cm telescope through a 15 arcsec diaphragm using the Bochum single channel photometer and an EMI 9558A photomultiplier tube. The observational procedure and reduction process were the same as those used at other telescopes. Johnson *JHKLM* photometry was obtained in January 1984 at the ESO 1 m telescope for 4 ROX optical counterparts (ROXs 6, 8, 29, and 47A). The observational procedure and reduction process are described in Bouvier *et al.* (1988).

3. Results.

3.1. SPECTROSCOPIC PROPERTIES OF THE OPTICAL COUNTERPART CANDIDATES.

Figure 2 displays the low- and medium-resolution spectrograms of the optical counterpart candidates ordered by increasing ROX source number. The spectrograms of stars with strong emission lines were plotted twice on different intensity scales to show both the spectral continuum and the line strength. For flux-calibrated spectrograms, the ordinate is in units of 10^{-16} erg s^{-1} cm^{-2} Å^{-1}. Otherwise, the stellar continuum was normalized to unity. The signal-to-noise ratio is a few tens for most spectrograms though the faintness of some stars, especially at short wavelengths, coupled with the poor efficiency of the IDS detector below 4000 Å sometimes results in a poor signal-to-noise ratio shortwards of 4200 Å.

Spectral types and equivalent widths of the major emission lines (Hα, Hβ, Ca II H-K) are listed in Table 4. Spectral classification was done by comparing the spectrograms of the stars with those of spectroscopic standards obtained under the same conditions. Only 3 stars have a spectral type earlier than G0, while 37 have a spectral type in the range from K0 to M5. The primary criterion used for the spectral classification of late K and M stars was the appearance and relative depths of TiO bands in the 5500-7700 Å spectral region. The depth of TiO band is extremely sensitive to effective temperature in this temperature range, so that the spectral type is derived with an accuracy of ± 1 subclass. The spectral classification of early- and mid-K stars in the blue range mainly rests upon the strength of the Ca I λ4226 line compared to that of the neighboring *G*-band of CH λ4290-4314. Spectral types derived in this way are accurate to within 1 subclass. The spectral type of early- and mid-K stars with strong emission lines (e.g., ROXs 6, ROXs 44) was deduced from red spectrograms with an accuracy of ± 2 subclasses. Except for a few striking cases (see below), spectral types derived from blue and red spectrograms usually agree to within 1 subclass. Due to the paucity of spectroscopic templates, classification of stars with a spectral type earlier than K0

© European Southern Observatory • Provided by the NASA Astrophysics Data System

1992A&AS...92..481B

may be uncertain by up to several subclasses. In this case, a ":" is appended to the spectral type given in Table 4. Finally, some spectrograms had too low a signal-to-noise ratio to reliably assign a spectral subclass. The spectral type of these stars is followed by "?" in Table 4.

The Hα emission line equivalent width (column 3) was measured above a linear interpolation of the adjacent continuum. No allowance was made for the underlying photospheric absorption profile whose equivalent width can amount to a few Å in late-type dwarfs. For strong emission line stars (EW(Hα) > 10 Å), the uncertainty is less than 20% but is may reach up to a factor of 2 for EW(Hα) of a few Å, especially when measured on low-resolution spectrograms. When the Hα line was seen neither in emission nor in absorption, it was assumed that the photospheric profile is filled-in by emission, and an "f" is given in Table 4. It should be noted that Hα emission-lines with an equivalent width less than 2 Å are usually not detected on low-resolution spectrograms, though easily seen at medium spectral resolution. Finally, when significant time variations of the Hα equivalent width occurred, the extreme observed values are listed in Table 4 followed by "(v)". Hβ, Ca II K, and Ca II H + Hϵ equivalent widths (columns 4 to 6) were measured only when the lines unambiguously appear in emission or in absorption (a positive equivalent width in Table 4 indicates an emission-line). When emission merely appears as a reversal in the core of the Ca II photospheric absorption line, the equivalent width was measured above the continuum interpolated between the base of the photospheric profile.

The presence of the Li I λ6707 line in absorption provides a strong clue for stellar youth in late-type stars since lithium is rapidly depleted on the main sequence. Therefore, this feature is very useful to differentiate between ρ Ophiuchus cloud members and field stars in our sample. Unfortunately, the equivalent width of this line does not exceed a few tenth of an Å in young stars, which is too small to be reliably measured on the spectrograms presented here. However, because this line provides a primary criterion to assess cloud membership, it was searched for in all the spectrograms. On medium-resolution spectrograms, the λ6707 Li I line can be easily distinguished from the neighboring λ6717 Ca I line. At lower resolution, however, the Li I/Ca I blend increases and the identification of the lithium line becomes more uncertain. We estimated that a lithium line with an equivalent width less than 0.3 Å cannot be detected on our low-resolution spectrograms. The results are listed in column 7 of Table 4: "y" means that the line was seen in absorption while "n" indicates that it was not detected. In case of possible confusion between the Li I and Ca I lines, ":" is appended to the result. Finally, when the spectrogram has too low a signal-to-noise ratio to decide whether the line is present or not, "?" is given in Table 4.

In addition to the spectroscopic survey, four optical counterpart candidates (ROXs 3, 21, 29, 44), known to be pre-main sequence cloud members, were monitored for spectral variations in the 5500-7500 Å range on a night-to-night basis between June 10 and June 21, 1985. The spectrograms are shown in Figure 3a)-d) and Hα equivalent width measurements are listed in Table 5. The surface of two stars, ROXs 21 (= SR 12) and ROXs 29 (= SR 9), was known to be covered with large, cool starspots (Bouvier & Bertout 1989) and the aim of the spectroscopic monitoring was to search for a link between spectral characteristics variations and spot's visibility. Although the spectrograms were obtained over a time period covering several rotational cycles for both ROXs 21 ($P_{\rm rot}$ = 3.4 d) and ROXs 29 ($P_{\rm rot}$ = 6.4 d), no significant variations of the photospheric spectrum are seen. The lack of detectable changes in the TiO band depth of these M stars indicates that spectral type variations did not exceed 1 subclass during the whole observational period. Similarily, the photospheric spectrum of the two other stars, whose rotational periods, however, are unknown, remained unchanged. In contrast, significant night-to-night variations of the Hα equivalent width occured. For instance, the Hα equivalent width of ROXs 29 increased from 12.2 to 26.1 Å from one night to the other. We find, however, no evidence for a periodic behaviour in the variations of the Hα line strength that could be related to the visibility of surface spots. Apart from the Hα line, only the λ5876 He I line is clearly seen in emission in the spectrum of ROXs 44 (and marginally in the spectrum of ROXs 29). Although He I equivalent width measurements are uncertain due to the blend with the neighboring NaD lines at low spectral resolution, it appears that Hα and He I line variations are correlated.

3.2. Stars with peculiar spectra.

While the agreement between spectral types deduced from the blue and the red spectrograms is usually very good, some widely different results were obtained in a few cases. This is illustrated in Figure 4, where the blue and red spectrograms of three pre-main sequence cloud members, ROXs 3, 21, and 47A, are compared to those of spectroscopic standards having a spectral type K4, K7-M0, and M0, respectively. While the blue spectrograms of the 3 pre-main sequence stars clearly point to a spectral type K4 or even slightly earlier, the deep TiO bands seen in the red spectral region unambiguously indicate a spectral type M0 or later. The blue and red spectrograms of ROXs 3 were obtained two days apart, while those of ROXs 21 and ROXs 47A are separated by 15 days. Consequently, we cannot rule out the possibility that the effective temperature of the stars drastically changed over a period of a few days. However, as discussed above, we failed to detect any effective temperature variation for ROXs 3 and

© European Southern Observatory • Provided by the NASA Astrophysics Data System

1992A&AS...92..481B

ROXs 21 from red spectrograms obtained over 12 consecutive nights. This strongly suggests that the increasingly later spectral type as a function of wavelength is a real effect and not merely the result of temporal variations. Similar wavelength dependent spectral characteristics (always indicating an earlier spectral type in the blue spectral range) have already been found in other T Tauri star samples (e.g., Walker 1980, Appenzeller 1977, Appenzeller *et al.* 1983). However, the present data illustrate this effect particularly well.

We discuss below three possible explanations for the origin of such composite spectra, namely: i) the objects are unresolved binary systems, ii) the temperature distribution at the stellar surface is inhomogeneous due to the presence of either cool starspots or bright chromospheric plages, and iii) the emission from a shock-heated region near the stellar surface dominates the stellar flux in the blue spectral range. In order to get further constraints from the observations, we first tried to reproduce the observed spectra in the 4000-7200 Å range. A grid of composite spectra was constructed from the digital addition of the spectrograms of two standard stars, one having a spectral type between K0 and K4, and the other between M0 and M5. After several trials, we found that the synthetic spectrum which best approximates the observations is the sum of a K0 and a M1.5 spectrograms normalized to the same flux at 5500 Å. This spectrum is compared to the observed ones in Figure 5. The K0 component ($T_{\rm eff}$ = 5250 K) dominates in the blue spectral region while the contribution of the M1.5 component ($T_{\rm eff}$ = 3590 K) clearly appears at longer wavelengths. Although the synthetic spectrum does not provide a perfect fit to the observations, the agreement is good enough for the present purpose (note that the slope of the spectral continuum in the observed and synthetic composite spectra may not be compared since the former have not been corrected for reddening).

The most straightforward explanation for the observed composite spectra is that the objects are binary systems with the two stars having widely different effective temperatures. Indeed, Simon *et al.* (1987) found ROXs 21 (= *SR* 12) to be a binary system from lunar occultation observations with a projected separation of less than 0.2 arcsec. From the flux ratio of the two components at near-IR wavelengths, they derive an effective temperature of 5000 K for the primary star and of 2500 K for the low-mass companion. However, while the temperature of the primary star roughly agrees with that derived for the hot component of the synthetic spectra ($T_{\rm eff}$ = 5200 K), the cool companion has much too low an effective temperature to significantly contribute to the total flux of the system at optical wavelengths. The binary interpretation faces the additional difficulty that, according to our crude modelling of the composite spectra, the two components must have comparable luminosities at 5500 Å. The radius of the M1.5 star then has to be 3.7 times larger than that of the K0 star, which implies that the hot component is on the main sequence while the cold one is still in the T Tauri phase, an uncomfortably large age difference indeed for such a close binary system.

Alternatively, the composite spectra may arise from an inhomogeneous temperature distribution at the stellar surface. A cold starspot located at the surface of a K0 star and radiating like a 3590 K photosphere would have to cover 93% of the star's visible hemisphere in order to have the same luminosity than the remaining unperturbed photosphere at 5500 Å. This fractional area is unrealistically large compared to the usual properties of dark spots on pre-main sequence stars, which typically cover from 10 to 20% of the stellar surface (Bouvier & Bertout 1989). Conversely, a bright region with a temperature of 5250 K, e.g., a chromospheric plage, located at the surface of a M1.5 photosphere would only have to cover 7% of the stellar surface to yield the same result. As empirically shown by Finkenzeller & Basri (1987) and Appenzeller *et al.* (1986), the emission from such a chromospheric region would differentially affect photospheric line profiles. Lines of low-excitation potential which form in the upper photosphere may be significantly filled-in by chromospheric emission, while those which arise in the deep photosphere are essentially unaffected. They further showed that the differential veiling of photospheric lines by chromospheric emission is more apparent in the blue spectral region than in the red one. In contrast to the atomic lines, the TiO bands used for spectral classification in the red will be much less affected by chromospheric emission as the molecular species cannot exist in the hot, rarefied chromospheric layers. Therefore, spectral types deduced from blue spectrograms may be largely in error if the relative intensities of photospheric lines are affected by chromospheric veiling. This, however, may not be the case for the stars considered here because, as indicated by their faint Ca II H and K emission features, they possess very weak chromospheres. In comparaison, all the pre-main sequence stars included in Finkenzeller & Basri's study have much stronger Ca II H and K emission peaks. Yet, none shows evidence for spectral type variations as a function of wavelength.

Since ROXs 3, 21, and 47A are found below to be young, low-mass stars embedded in the cloud, the possibility that these stars possess circumstellar disk from which they might accrete material must be contemplated. One of the clearest signature of the presence of optically thick circumstellar disks around pre-main sequence stars is the near-IR continuum flux excess which results from the thermal emission of circumstellar material near the stellar surface (e.g., Kenyon & Hartmann 1987, Bertout *et al.* 1988). Quasi-simultaneous visual and near-IR photometry was only obtained for ROXs 47A which is found to exhibit a continuum excess of a few tenth of a magni-

© European Southern Observatory • Provided by the NASA Astrophysics Data System

1992A&AS...92..481B

tude at near-IR wavelengths. We also note that ROXs 21 has been detected at near- and far-IR wavelengths (Wilking *et al.* 1989). Part of the infrared excess, however, may be due to the presence of a low-mass companion (Simon *et al.* 1987). No near-IR photometry is available for ROXs 3. A major clue for disk *accretion* comes from the optical excess which arises in the accretion boundary layer located at the interface between the star and the disk. This excess is usually referred to as optical veiling since its major consequence is to fill-in the photospheric line profiles with continuous emission. Optical veiling correlates with Hα emission strength (Hartigan *et al.* 1990) and is easily seen in the high-resolution spectrograms of strong emission-line T Tauri stars which accrete from their disk at a rate of typically 10^{-7} $M_\odot$ yr^{-1} (e.g., Basri & Batalha 1990, Hartigan *et al.* 1990). In contrast, the lack of detectable optical veiling in the medium-resolution spectrograms of the stars studied here sets an upper limit of a few 10^{-8} $M_\odot$ yr^{-1} on the mass-accretion rate (see Basri & Bertout 1989). Similarly, the weak Hα emission these stars display suggests that, if accretion actually occurs, it must proceed at a somewhat reduced rate.

Obviously, the spectral characteristics of ROXs 3, 21, and 47A do not provide compelling evidence for disk accretion, though they may still be consistent with low accretion rates. Since alternative explanations of the observed composite spectra are unsatisfactory, we feel that it is worth investigating this possibility further. If entirely derived from the kinetic energy released in the accretion boundary layer, the luminosity of the blue component in the observed composite spectra points to a mass-accretion rate of approximately 4 10^{-8} $M_\odot$ yr^{-1}. Alternatively, if the luminosity of the red component resulted from viscous energy dissipation in the inner disk regions, a much larger accretion rate would be required and would result in significant optical veiling and line-emission. Since the observed spectra show no evidence for veiling and have only weak line emission, we will assume in the following that the red component corresponds to the photosphere of a M1.5 pre-main sequence star while the K0 component seen at shorter wavelengths is related to the accretion process.

According to classical disk models, accretion of disk material at a rate of 4 10^{-8} $M_\odot$ yr^{-1} at the surface of a M1.5 pre-main sequence star results in a black-body temperature of the order of 8000 K for the boundary layer and 3000 K or less for the inner disk regions (see, e.g., Basri & Bertout 1989). Hence, even though the accretion luminosity is then sufficient to account for the luminosity of the blue component, neither the boundary layer nor the inner disk regions are expected to mimic a K0 photosphere. None of the accretion disk models developed so far, however, take into account the heating of the inner disk regions by the hot boundary layer. Presumably, some of the boundary layer luminosity is lost to this process, thus leading to a somewhat higher temperature in the inner disk regions than predicted by current disk models. An intriguing possibility is that the K0 component of the composite spectrum arises from the photosphere of the inner disk regions whose temperature has been increased by this process.

There are some obvious difficulties with this interpretation. One is that a very significant fraction of the boundary layer luminosity must be intercepted by the inner disk in order for the disk photosphere to have the same flux than the star at 5500 Å. Another is that, to our knowledge, there has been no report of optical composite spectra (at least not at the level observed here) for T Tauri stars which accrete from their disk at a rate in excess of 10^{-7} $M_\odot$ yr^{-1} (with the exception of FU Orionis objects where the star's luminosity is completely masked by disk emission, see, e.g., Hartmann & Kenyon 1985). Furthermore, all *bona fide* T Tauri stars observed so far with high spectral resolution show in all spectral ranges absorption line profiles fully consistent with those expected from slowly rotating stellar photospheres without significant contributions by a rapidly rotating inner Keplerian disk. Therefore, until more convincing evidence is produced for the presence of accretion disks around the stars considered here, and pending a consistent modelling of the heating of the inner disk regions by the accretion boundary layer, we see this interpretation of the observed composite spectra as being highly speculative.

As a further possibility for explaining the effective temperature discrepancy we note that it could be caused by small but hot and bright infall-heated regions of the T Tauri photosphere. High-resolution emission line profiles of T Tauri stars suggest that at least part of these objects have more or less extended "free-fall zones" between the inner edge of their accretion disks and the photosphere (e.g., Krautter *et al.* 1990). These free-fall zones seem to be caused by magnetic fields corotating slowly with the central star, preventing stable Keplerian disk rotation inside the corotation radius (e.g., Camenzind 1990). Accretion inside the corotation radius presumably occurs along the magnetic lines of force, resulting in localized shock-heating of regions near the stellar surface. This explanation was put forward by Bertout *et al.* (1988) in order to explain the existence of a small but hot spot at the surface of the T Tauri star DF Tauri. Photospheric hot spots originating from this local heating could possibly give rise to the earlier spectral characteristics of the blue light emitted from there.

A wavelength-dependent spectral type is also suggested for ROXs 2 and, perhaps, ROXs 29. The low-resolution spectrogram we obtained for ROXs 2 extends from 5500 to 7700 Å. A spectral type of K3 is deduced from the spectral region bluewards of Hα, while the presence of a TiO band between 7050 and 7200 Å suggests M0. The discrepancy between the spectral types deduced

© European Southern Observatory • Provided by the NASA Astrophysics Data System

1992A&AS...92..481B

from blue (K4) and red (K6) spectrograms of ROXs 29 is barely significant.

3.3. PHOTOMETRIC PROPERTIES OF THE OPTICAL COUNTERPART CANDIDATES.

Table 6 lists the photometric properties of the optical counterpart candidates. Some were repeatedly observed in the *UBVRI* Cousins system in which case only the mean V, $B-V$, $U-B$, $V-R_c$, and $V-I_c$ colors are listed in Table 6, while individual measurements are given in Table 7 if not published elsewhere. Extensive optical photometry was published in Bouvier *et al.* (1988) for ROXs 3, 6, 8, 21, 29, 34, 44, and 47A. For stars with no photometric measurements, the V magnitude was derived from flux calibrated spectrograms when available and the $B-V$, $V-R_c$, and $V-I_c$ colors from the continuum slope of low-resolution spectrograms, whether flux calibrated or not. Magnitudes and colors derived in this way appear within parentheses in Table 6. The uncertainty of the spectroscopically derived V magnitude is of 0.4 mag (compared to 0.02 mag for photometric measurements), while colors are uncertain by approximately 0.2 mag. The results of *JHKLM* photometry obtained for ROXs 6, 8, 29, and 47A are given in Table 8.

Column 7 of Table 6 lists the visual extinction on the line of sight computed from the $(V-R)$ color excess assuming a standard extinction law ($A_v = 3.81 \cdot E[V-R]$). The Cousins' $(V-R)$ index was first transformed to Johnson's $(V-R)$ using Fernie's (1983) relationships. Then, the $(V-R)$ color excess was obtained by subtracting the intrinsic $(V-R)$ index of a dwarf having the same effective temperature (Johnson 1966). This procedure assumes that the color excess is entirely due to reddening, an assumption which should hold at least for weak emission-line stars which constitute the vast majority of our sample (see Strom *et al.* 1989). In strong emission-line stars, however, the $(V-R)$ index may be affected in a complex way by continuum emission arising from a circumstellar disk and the associated accretion boundary layer. Hence, while the error on the visual extinction is estimated to lie within 0.3 mag for weak emission-line stars, its derivation is more uncertain for strong emission-line stars.

The stellar luminosity (column 8) was derived from the dereddened V magnitude applying bolometric corrections listed by Johnson (1966) for dwarfs and assuming a distance of 170 pc for the ρ Ophiuchus cloud (see Carrasco *et al.* 1973, and references therein). De Geus *et al.* (1989) recently derived a distance of 125 ± 25 pc for the cloud from a spectrophotometric study of early-type stars belonging to the Upper-Scorpius OB association. In that case, the luminosities listed in Table 6 are reduced by 0.27 dex. The luminosity of strong emission-line stars may be systematically overestimated by as much as a factor of 2 due to the contribution of an accretion boundary layer to the observed flux in the V-band (Kenyon & Hartmann 1990). However, the adopted procedure should provide a reliable estimate of the true stellar luminosity of weak emission-line stars.

4. Discussion.

4.1. CLOUD MEMBERSHIP.

All the stars studied here are projected against the ρ Ophiuchus dark cloud. Unfortunately, we lack radial velocity measurements to unambiguously assess membership. We used the following primary criteria to identify young members of the cloud: the Li I λ6707 line is present in absorption in the spectrum and the Hα line appears in emission above the continuum. While the former criterium provides strong evidence for stellar youth, the latter is more ambiguous. On the one hand, not all pre-main sequence stars show Hα in emission (see, e.g., Walter *et al.* 1989), and, on the other, late-type active main-sequence stars such as dKe and dMe stars exhibit a faint Hα emission line, with an Hα equivalent width up to 5 Å (Stauffer & Hartmann 1986). Therefore, only stars which have an Hα equivalent width larger than that of active dwarfs of the same spectral type can be confidently classified as pre-main sequence cloud members. When the results obtained from these two criteria are inconclusive, secondary criteria may be helpful. For instance, the presence of a near-IR excess suggests membership while significant visual absorption indicate that the star is either embedded within the cloud or lie beyond it. Similarly, the far-IR or radio properties of some stars in our sample sometimes provide additional clues to their youth. In the following, we discuss the probability that the observed stars are cloud members based on these criteria.

The following stars exhibit Hα in emission: ROXs 2, 3, 4, 5, 6, 7, 10A, 10B, 12, 16, 20A, 20B, 21, 29, 30B, 30C, 31, 33, 34, 39, 42B, 42C, 43A, 43B, 44, 45F, 47A. Except for ROXs 4, 20A, 20B, 31, 33, and 42B, these stars also have lithium absorption, which leaves no doubt as to their pre-main sequence status. The lithium line was only marginally detected in ROXs 4, 33, and 42B and could not be seen in the low-resolution spectrogram of ROXs 31. Nevertheless, ROXs 4, 20B, 31, and 33 can be unambiguously classified as pre-main sequence stars on the basis of their strong Hα emission compared to that of active dwarfs of similar spectral types. Moreover, all four stars have possible near- or far-IR counterparts (see Table 2). Interestingly enough, Struve & Rudkjøbing (1949) found ROXs 33 (= SR 20) to be a non-emission line star, while, 10 years later, Dolidze & Arakelyan (1959) detected strong Hα emission (= DoAr 38). We measured an Hα equivalent width of 21 Å for this star, and the Hα line exhibits a well-developed P Cygni profile. The non-detection of the lithium line in the low-resolution spectrogram of

© European Southern Observatory • Provided by the NASA Astrophysics Data System

1992A&AS...92..481B

such a late-type star as ROXs 20 A (Sp = M5) does not constitute a strong evidence against pre-main sequence status because the line is located within deep TiO and CaH bands, and thus difficult to detect. In fact, ROXs 20 A suffers strong visual extinction (A_v = 2.6 mag) and since its luminosity is far too large to be compatible with that of a background dM5e star, we conclude that it is a cloud member. Its proximity to ROXs 20B (projected separation of 10") suggests they form a physical pair (see Sect. 4.3). Similarly, ROXs 42B has only faint Hα emission, with EW(Hα) = 1.7 Å, but its high visual extinction (A_v = 2.5 mag) and large stellar luminosity suggest that it is embedded within the cloud.

ROXs 8, 14 and 45 E are most likely additional cloud members, even though no Hα emission is seen above the continuum in their spectrum. ROXs 8 displays a strong lithium line, and, while Hα now appears as a faint absorption feature, it was previously detected in emission by Dolidze & Arakelyan (1959). It also has strong near- and far-IR excesses and has been detected in the radio range at 1.4 and 5 GHz (see references in Table 2). ROXs 14, a B4 star, exhibits strong Hα absorption and no lithium absorption, as expected for such a massive star. Nevertheless, it suffers strong visual extinction (A_v = 10.3 mag) which indicates that it is either a background object or a young massive star deeply embedded within the cloud. Since it is projected against the central regions of the cloud where the gas column density is very high ($A_v > 50$ mag), the former possibility is very unlikely. Moreover, radio observations at 5 GHz showed that the star excites a compact HII region whose age is estimated to be of the order of 5 10^3 yr (André *et al.* 1988). Finally, the Hα line of ROXs 45E seems to be filled-in by emission but the signal-to-noise ratio is too low to investigate lithium absorption. It might be a foreground dKe star since its visual extinction is negligeable (A_v = 0.1 mag). However, the close proximity of ROXs 45E and 45F, the latter being identified above as a pre-main sequence star, as well as their similar properties, suggest that they form a physical pair. Moreover, ROXs 45E and 45F seem to coincide with the stars # 49 and # 50 of Dolidze & Arakelyan's (1959) Hα survey, which were both found to exhibit faint Hα emission at that time.

A total of 30 stars are identified above as certain cloud members. An additional cloud member may be ROXs 45D since its position coincides with that of Dolidze & Arakelyan's (1959) Hα emission-line star # 48, though Hα now appears in absorption. The 16 remaining stars have either Hα in absorption or no apparent Hα feature and no lithium line is seen in their low-resolution spectra. Except for ROXs 35B, none of them have been detected at other wavelengths (most of them, however, lie in areas of the cloud not covered by previous near- and far-IR studies). ROXs 36 (HD 148562) has a low visual extinction (A_v = 0.4 mag) and was classified as a main sequence member of the Upper Sco-Cen association by Garrison (1966). ROXs 35B and ROXs 47B suffer insignificant extinction ($A_v \leq 0.2$ mag) and are most likely foreground dwarfs. The 13 other stars, however, are strongly reddened with a visual extinction between 1.5 and 4.5 mag, which indicates that they are either cloud members or background objects.

We believe that most, perhaps all, of these stars are late-type background giants (they have too high a stellar luminosity to be background dwarfs). Although a luminosity class cannot be confidently assigned from the low-resolution spectrograms of these stars, several lines of evidence support this hypothesis. In contrast to most cloud members identified above, the non emission-line stars are projected against the very edge of the cloud where the ^{13}CO gas column density is quite low (Loren 1989), so that background objects can easily be seen. Moreover, these stars have a higher visual extinction than identified cloud members on adjacent lines of sight, as expected for background objects. Finally, non-emission line stars which lie in the same X-ray error circle suffer comparable visual extinction (see, e.g., ROXs 9A, 9B, 9C, 9D), which further suggests that they all lie behind the cloud.

Nevertheless, we note striking similarities between the spectral properties of these non emission-line stars and those of some X-ray emitting, pre-main sequence stars in the Taurus-Auriga cloud. In a similar study, Walter *et al.* (1989, hereafter WBMMV) found that a number of X-ray sources in the Taurus-Auriga region are young, late-type stars which have Hα in absorption on low-resolution spectrograms. While WBMMV classified them as cloud members on the basis of radial velocity measurements, Hartmann *et al.* (1990) concluded from a proper motion study that some may actually be low-mass members of the nearby Cassiopeia-Taurus B star group. Both studies agree, however, that these stars have an age less than a few 10^7 yr. WBMMV note that all the non emission-line stars in their sample have a spectral type K5 or earlier, and argue that the lack of Hα emission above the continuum is due to the presence of a deep underlying Hα photospheric profile. Similarly, all the stars that have Hα in absorption in our sample have a spectral type K6 or earlier, except for ROXs 9A, an M0 star. Moreover, the non emission-line stars of WBMMV's sample have lithium equivalent widths of 0.3 Å or less, which would be difficult to detect in our low resolution spectrograms. Finally, WBMMV found the non emission-line stars to be located in low-density parts of the cloud, much like the non-emission line stars in our sample.

Clearly, in the absence of radial velocity measurements, we are unable to assign a definite status to the non emission-line stars in our sample. If membership is assumed, their location in the HR diagram (not shown) indicates ages ranging from a few 10^6 to a few 10^7 yrs. In turn, this would imply that star formation has been

© European Southern Observatory • Provided by the NASA Astrophysics Data System

1992A&AS...92..481B

an ongoing process in the ρ Ophiuchus cloud for a few 10^7 yr.

4.2. THE ROX OPTICAL COUNTERPARTS.

Of the 29 *Einstein* IPC error circles investigated here, 24 contain at least one pre-main sequence (pms) star, sometimes two. This confirms the suggestion of MKFG that most ROX sources are young cloud members. The maximum count rate in the 0.2 – 4 keV range quoted by MKFG for the 5 remaining sources (ROX 9, 35, 36, 38, and 40) is a factor 2 to 4 lower than the average maximum count rate for pms stars. Their optical counterparts may be either main sequence stars or background sources, as discussed below:

ROX 9: we observed 4 stars lying more than 2 arcmin away from the center of the error circle. All are late-type, non emission-line stars. The optical counterpart may be one of the much fainter objects located closer to the circle center.

ROX 35: one of the two observed stars, ROXs 35A, a non emission-line K3 star, lies right at the center of the error circle and is probably the optical counterpart of the X-ray source. The other, ROXs 35B, a G4 foreground field dwarf, lies 3 arcmin away. Two other stars located near the center of the error circle were too faint to be included in this study.

ROX 36: the center of the X-ray circle coincides with HD 148562, a young main sequence member of the Upper Sco-Cen association according to Garrison (1966).

ROX 38: two stars, ROXs 38A and 38B, are located 88 and 28 arcsec away from the center of the error circle. Both are late-type stars and plausible optical counterparts.

ROX 40: ROXs 40, a K6 star, lies 3 arcmin from the center of the X-ray circle. A faint object is located approximately 30" away from ROXs 40, for which we obtained a very low quality spectrum which shows no evidence for Hα emission. Several fainter stars are located closer to the error circle center.

Of the 30 pms X-ray sources identified here, 17 were detected in previous Hα surveys of the cloud (Struve & Rudkjøbing 1949, Doldze & Arakelyan 1959, Wilking *et al.* 1987). Most of them are also near- or far-IR sources and a few have been detected in the radio range at 1.4 and 5 GHz (see Table 2). We used the bolometric luminosities derived above and the effective temperature deduced from the spectral type using the Sp – $T_{\rm eff}$ scale given by Cohen & Kuhi (1979) to construct and HR diagram for these pre-main sequence cloud members. The HR diagram is shown in Figure 6 and contains more than twice as many stars as the previous one presented for this cloud (Cohen & Kuhi 1979). Only ROXs 14, for which we have no luminosity estimate, does not appear in this figure. However, Lada & Wilking (1984) found that ROXs 14 has a dereddened IR spectral energy distribution similar to that of a ZAMS dwarf of spectral type B3-B5. This is in agreement with the spectral type of late B derived from a low-resolution optical spectrogram by Grasdalen *et al.* (1973, Source 1) and with radio data which indicate that ROXs 14 is a young, massive member of the cloud (André *et al.* 1988).

As expected for young cloud members, all the stars in Figure 6 lie well above the main sequence. According to the theoretical isochrones given by Cohen & Kuhi (1979), their age ranges from $\simeq 10^6$ to 10^7 yr and their mass from 0.3 to 2.7 $M_\odot$. Histograms of spectral types, stellar masses, and Hα equivalent widths are shown in Figure 7. Most of the stars have a spectral type K or early M. In fact, the age, mass, and spectral type distributions of ROX sources are quite similar to those of *bona fide* T Tauri stars in the Taurus-Auriga cloud (see Cohen & Kuhi 1979). Unlike the Taurus-Auriga T Tauri stars studied by Cohen & Kuhi, however, most of the optical counterparts of the ROX sources are weak emission-line stars ($EW(\mathrm{H}\alpha) < 10$ Å). Only 9 X-ray sources (ROXs 6, 10A, 16, 29, 30B, 30C, 33, 34, 44) are classical T Tauri stars with $EW(\mathrm{H}\alpha) \geq 10$ Å and all have been detected at near- or far-IR wavelengths.

In a similar study, WBMMV identified a number X-ray sources in the Taurus-Auriga molecular cloud as being "naked" T Tauri stars, i.e., weak emission-line pms stars with no near-IR excess. They went on to suggest that naked T Tauri stars outnumber classical T Tauri stars by a factor of 10 in the Taurus-Auriga cloud. Among the 20 weak-line ROX optical counterparts, only 9 (ROXs 3, 5, 12, 39, 42B, 42C, 43A, 45E, 45F) have optical and IR properties similar to those of WBMMV's naked T Tauri stars. The 11 remaining weak emission-line stars (ROXs 2, 4, 7, 8, 10B, 20A, 20B, 21, 31, 43B, 47A) were detected at near- or far-IR wavelengths, which points to a significant IR excess. Thus, while the ratio of weak- to strong-emission line stars is close to 2:1 in our sample, we find an approximately equal number of classical and naked T Tauri stars. If the 18 ROX sources not investigated in the present study turned out to be naked T Tauri stars, the ratio of naked to classical TTS in the X-ray population of the ρ Ophiuchus cloud would be 3:1. These figures are similar to those derived for X-ray sources in the Chameleon and Lynds 1641 dark clouds (Feigelson & Kriss 1989, Strom *et al.* 1990).

As far as their evolutionary status is concerned, the ROX sources form an homogeneous population of low-mass, pms stars (with the exception of ROXs 14, a young, massive B star). Moreover, they span a relatively limited range of X-ray luminosity, from 10^{30} to a few 10^{31} erg s^{-1} (MKFG). This strongly contrasts with the wide range of spectral properties they display at other wavelengths. The sample includes both weak- and strong-emission line stars, some of which are strong near-IR or *IRAS* sources while other have no IR excess, and some ROX sources are radio emitters although the majority are not detected

© European Southern Observatory • Provided by the NASA Astrophysics Data System

1992A&AS...92..481B

at radio continuum wavelengths. Clearly, X-ray emission is not the privilege of a subclass of visible pms stars with well-defined spectral properties. On the contrary, X-ray emission appears to be largely independent of the spectral properties of the stars at other wavelengths. It is commonly believed that X-ray emission in these stars is a manifestation of solar-like, magnetic surface activity (MKFG, WBMMV, Bouvier 1990, Strom *et al.* 1990). In contrast, strong IR excesses and line-emission are thought to be related to the accretion of material from a circumstellar disk at the stellar surface (e.g., Kenyon & Hartmann 1987, Bertout *et al.* 1988, Basri & Bertout 1989, Cabrit *et al.* 1990). The lack of a correlation (or an anti-correlation) between the X-ray properties and IR excess or Hα emission of young, visible stars in the ρ Ophiuchus cloud is fully consistent with the view that distinct physical mechanisms are responsible for these properties.

4.3. The close optical pairs.

Six X-ray error circles contain pairs of emission-line stars: ROX 10, 20, 30, 42, 43, and 45. In each case, the two stars are probably X-ray emitters but the spatial resolution of *Einstein* IPC frames is too low to separate their relative contributions. Although it is difficult to decide whether these close optical pairs are true binary systems in the absence of radial velocity measurements, their properties are reviewed below and the likelihood of physical association discussed:

ROXs 10A, 10B: according to their position in the HR diagram, the two stars have similar ages (approximately 10^6 yr) but widely different masses (1.3 and 2.3 $M_\odot$, respectively). The separation of 94" at P.A. = 113° makes physical association unlikely. Moreover, ROXs 10B suffers much stronger extinction than ROXs 10A (A_V = 6.6 and 3.3 mag, respectively). From IR speckle observations, Chelli *et al.* (1988) found ROXs 10B (= DoAr 24E) to have a low-mass, infrared companion at a distance of 2.3 arcsec at P.A. = 30 ± 10°.

ROXs 20A, 20B: two M stars with weak Hα emission separated by 10" at P.A. = 126°. While they have similar masses (0.4 and 0.3 $M_\odot$, respectively), their location in the HR diagram suggests that they have widely different ages. The two stars suffer quite different amounts of visual extinction (A_V = 2.6 and 0.7 mag, respectively), which is surprising for such a close optical pair. If a physical system, most of the extinction towards ROXs 20A must be of circumstellar origin.

ROXs 30B, 30C: the separation is 48" at P.A. = 170°. The two stars have very similar properties (spectral type, mass, age, Hα equivalent width), and comparable extinction values, which suggests that they form a wide binary system.

ROXs 42B, 42C: the two stars have similar ages according to their position in the HR diagram but widely different masses and spectral types. The separation of 77" at P.A. = 174° casts doubt upon their physical association. ROXs 42C is a double-lined spectroscopic binary with a period of 35.95 days (Mathieu *et al.* 1989).

ROXs 43A, 43B: with a separation of 6" at P.A. = 13°, the two stars are hardly separated on POSS red prints. Although they have quite different spectral types and luminosities, their similar age suggests they form a close physical system. Mathieu *et al.* (1989) found ROXs 43A to be a single-lined spectroscopic binary with an orbital period of 89.1 days.

ROXs 45E, 45F: located 15" apart at P.A. = 75°, the two stars have similar properties and lie at the same position in the HR diagram. In fact, we classified ROXs 45E as a cloud member partly on the basis of its assumed physical association with ROXs 45F.

In addition to the above optical pairs, ROXs 21 (= *SR* 12) and ROXs 31 were found to be sub-arcsecond binaries by Simon *et al.* (1987) from lunar occultation observations. Both systems have also been resolved at near-IR wavelengths by speckle observations (Zinnecker & Perrier 1988).

5. Summary and conclusions.

Of the 47 stars included in this study, 30 were identified as being the pre-main sequence optical counterparts of 24 X-ray sources in the ρ Ophiuchus dark cloud. Most X-ray sources are weak emission-line stars that have an evolutionary status similar to that of *bona fide* T Tauri stars in the Taurus-Auriga stellar formation region. These results confirm the ability of X-ray surveys of star-forming regions to reveal pre-main sequence stars which might have escaped detection at other wavelengths. Indeed, while some X-ray sources are detected at infrared or radio wavelengths, the X-ray population of the cloud, as a whole, is distinct from the populations of infrared or radio sources.

Although the spectral properties of the 17 remaining stars of our sample provide no compelling evidence for membership, they bear strong similarities with weak-line pre-main sequence stars discovered during X-ray surveys of other stellar formation regions. If cloud members, these stars are significantly older than the emission-line stars, implying that star formation has been lasting for several 10^7 years in the ρ Ophiuchus cloud.

Acknowledgements.

It is a pleasure to thank C. Bertout who initiated the study presented here. We gratefully acknowledge many interesting discussions with T. Montmerle and Ph. André on the X-ray and radio properties of young stars in the ρ Ophiuchus cloud. They also suggested several improvements on an early version of the manuscript. We are indebted to P. Bouchet who obtained near-infrared pho-

© European Southern Observatory • Provided by the NASA Astrophysics Data System

1992A&AS...92..481B

tometry for 4 ROX optical counterparts and to C. Bertout who conducted the spectroscopic observations during the May 1986 run. The generous allocation of observing time by the ESO Program Committee and the competent technical support of ESO staff at La Silla are gratefully acknowledged. We also wish to thank Professor Rufener for permitting a long observing run at the La Silla Swiss telescope and M. Burnet for his help during the observations. One of us (J.B.) is grateful to F. Sevres for his assistance during the measurements of stellar positions with the $X-Y$ measuring machine of Institut d'Astrophysique de Paris and to Dr. Grosbol for his help during the digitalization of photographic plates at ESO Garching.

References

André Ph. 1987, in "Protostars and Molecular Clouds", ed. T. Montmerle & C. Bertout, (Saclay: CEA/Doc), p.143
André Ph., Montmerle T., Feigelson E.D. 1987, AJ 93, 1182
André Ph., Montmerle T., Feigelson E.D., Steppe H. 1990, A&A 240, 321
André Ph., Phillips R.B., Lestrade J.-F., Klein K.-L. 1991, ApJ, in press
André Ph., Montmerle T., Feigelson E.D., Stine P.C., Klein K.L. 1988, ApJ 335, 940
Appenzeller I. 1977, A&A 61, 21
Appenzeller I., Jankovics I., Jetter R. 1986, A&AS 64, 65
Appenzeller I., Jankovics I., Krautter J. 1983, A&AS 53, 291
Basri G., Batalha C. 1990, ApJ 363, 654
Basri G., Bertout C. 1989, ApJ 341, 340
Bertout C., Basri G., Bouvier J. 1988, ApJ 330, 350
Bouvier J. 1990, 99, 946
Bouvier J., Bertout C. 1989, A&A 211, 99
Bouvier J., Bertout C., Bouchet P. 1988, A&AS 75, 1
Cabrit S., Edwards S., Strom S.E., Strom K.E. 1990, ApJ 354, 687
Camenzind M. 1990, Rev. Mod. Astron., Vol.4, in press
Carrasco L., Strom S.E., Strom K.M. 1973, ApJ 182, 95
Chelli A., Zinnecker H., Carrasco L., Cruz-Gonzalez I., Perrier C. 1988, A&A 207, 46
Chini R. 1981, A&A 99, 346
Cohen M., Kuhi L.V. 1979, ApJS 41, 743
de Geus E.J., Bronfman L., Thaddeus P. 1990, A&A 231, 137
de Geus E.J., de Zeeuw P.T., Lub J. 1989, A&A 216, 44
Dolidze M.V., Arakelyan M.A. 1959, SvA 3, 434
Elias J.H. 1978, ApJ 224, 453
Feigelson E.D., Kriss G.A. 1989, ApJ 338, 262
Fernie J.D. 1983, PASP 95, 782
Finkenzeller U., Basri G. 1987, ApJ 318, 843
Garrison R.F. 1966, ApJ 147, 1003
Gliese W. 1969, Cat. Nearby Stars, Veröff Astron. Recheninstitut, Vol.22, Heildelberg
Grasdalen G.L., Strom K.M., Strom S.E. 1973, ApJ 184, L53
Haro G. 1949, AJ 54, 188
Hartigan P., Hartmann L., Kenyon S.J., Strom S.E., Skrutskie M.F. 1990, ApJ 354, L25
Hartmann L.W., Kenyon S.J. 1985, ApJ 299, 462
Hartmann L., Jones B.F., Stauffer J.R., Kenyon S.J. 1990, AJ 101, 1050
Herbig G.H., Bell K.R. 1988, Lick. Obs. Bull. No.1111
Ichikawa T., Nishida M. 1989, AJ 97, 1074
Johnson H.L. 1966, ARA&A 4, 193
Kenyon S.J., Hartmann L.W. 1987, ApJ 323, 714
Kenyon S.J., Hartmann L.W. 1990, ApJ 439, 197
Krautter J., Appenzeller I., Jankovics I. 1990, A&A 236, 416
Lada C.J., Wilking B.A. 1984, ApJ 287, 610
Leous J.A., Feigelson E.D., André Ph., Montmerle T. 1990, ApJ, submitted
Loren R.B. 1989, ApJ 338, 902
Loren R.B., Wootten A. 1986, ApJ 306, 142
Mathieu R.D., Walter F.M., Myers P.C. 1989, AJ 98, 987
Merrill P.W., Burwell C.G. 1950, ApJ 112, 72
Montmerle T., Koch-Miramond L., Falgarone E., Grindlay J.E. 1983, ApJ 269, 182 (MKFG)
Rydgren A.E. 1980, AJ 85, 438
Simon M., Howell R.R., Longmore A.J., Wilking B.A., Peterson D.M., Chen W.-P. 1987, ApJ 320, 344
Stauffer J.R., Hartmann L.W. 1986, ApJS 61, 531
Stine P.C., Feigelson E.D., André Ph., Montmerle T. 1988, AJ 96, 1394
Strom K.M., Strom S.E., Edwards S., Cabrit S., Strutskie M.F. 1989, AJ 97, 1451
Strom K.M., Strom S.E., Wilkin F.P., Carrasco L., Cruz-Gonzalez I., Recillas E., Serrano A., Seaman R.L., Stauffer J.R., Dai D., Sottile J. 1990, ApJ 362, 168
Struve O., Rudkjøbing M. 1949, ApJ 109, 92
Vrba F.J. 1977, AJ 92, 198
Vrba F.J., Strom S.E., Strom K.M. 1976, AJ 81, 958
Walker M.F. 1980, PASP 92, 66
Walter F.M., Brown A., Mathieu R.D., Myers P.C., Vrba F.J. 1989, AJ 96, 297 (WB-MMV)
Wilking B.A., Lada C.J. 1983, ApJ 274, 698
Wilking B.A., Lada C.J., Young E.T. 1989, ApJ 340, 823
Wilking B.A., Schwartz R.D., Blackwell J.H. 1987, AJ 94, 106
Young E.T., Lada C.J., Wilking B.A. 1986, ApJ 304, L45
Zinnecker H., Perrier C. 1988, ESO Messenger, No.51, p.31

© European Southern Observatory • Provided by the NASA Astrophysics Data System

1992A&AS...92..481B

TABLE 1. *Coordinates of ROX optical counterpart candidates.*

ROXs	R.A.(1950)	Dec.(1950)	ROXs	R.A.(1950)	Dec.(1950)
	h m s	° ′ ″		h m s	° ′ ″
2	16 22 23.5	-23 48 19	33	16 25 31	-24 16 06
3	16 22 47.6	-24 44 43	34	16 25 43.5	-24 21 42
4	16 22 48.7	-24 32 26	35A	16 26 31.5	-24 48 58
5	16 22 54.8	-23 48 23	35B	16 26 32.1	-24 45 53
6	16 22 54.7	-24 14 01	36	16 26 52.1	-24 52 15
7	16 22 55.9	-24 23 45	38A	16 27 12.4	-25 29 07
8	16 23 01.5	-24 16 49	38B	16 27 16.8	-25 29 43
9A	16 23 20.7	-25 40 33	39	16 27 33.6	-24 27 50
9B	16 23 27.5	-25 36 56	40	16 27 49.9	-24 05 06
9C	16 23 34.7	-25 38 30	42A	16 28 12.2	-24 27 50
9D	16 23 42.9	-25 39 02	42B	16 28 13.0	-24 26 19
10A	16 23 15.6	-24 13 36	42C	16 28 13.6	-24 27 36
10B	16 23 21.9	-24 14 13	43A	16 28 18.1	-24 23 40
12	16 23 25.2	-25 20 03	43B	16 28 18.2	-24 23 34
14	16 23 32.6	-24 16 43	44	16 28 31.5	-24 21 13
16	16 23 45.1	-24 05 15	45A	16 28 41.8	-25 24 05
20A	16 24 12.3	-24 44 51	45B	16 28 44.6	-25 25 09
20B	16 24 12.9	-24 44 57	45C	16 28 49.2	-25 23 58
21	16 24 17.5	-24 34 58	45D	16 28 54.5	-25 23 13
29	16 24 38.6	-24 15 23	45E	16 28 57.3	-25 24 07
30A	16 24 36.0	-23 52 53	45F	16 28 58.4	-25 24 03
30B	16 24 37.3	-23 50 50	47A	16 29 09.6	-24 33 59
30C	16 24 37.9	-23 51 37	47B	16 29 21.0	-24 33 58
31	16 24 50.1	-24 34 11			

Note: ROXs #n stands for ROXstar #n and indicates a visible star lying within the error circle of the X-ray source ROX #n. Stars lying in the same error circle have an arabic letter appended to their name, with the alphabetic order corresponding to increasing right ascension (see text).

© European Southern Observatory • Provided by the NASA Astrophysics Data System

1992A&AS...92..481B

TABLE 2. *Cross-identification list of ROX optical counterpart candidates.*

ROXs	Hα				Optical			Infrared					Radio		Notes
	SR	DoAr	WSB	Other	HBC	C	Other	GSS	VSS	EL	WLY	Other	AMF	SFAM	
2					635		MKFG		20						
3					636		MKFG								
4									23		IRS10				
6	4	20	25	AS 206	259	7	CK			13	IRS12, IRAS25	IRAS 16229-2413			1
7								20			IRS13, IRAS24				
8		21		Haro 1-6	637	10	MKFG	23	93	14	IRAS26		ROS4, ROC8	Src7	1, 2, 3
10A		24	27		638	14		28		19					2
10B		24E	30		639	16		31		22					2
14						19	CK	35 (S1)	26	25	IRAS36	IRAS 16235-2416	ROS8, ROC15	Src13	3, 4
16			38				MKFG		27		IRAS37?				
20A		31?	45		640		MKFG					MC16			
20B		31?	46		641		MKFG					MC16			
21	12				263		CK, R				IRS40	YLW13a			5, 6
29	9	34	54	AS 207	264	29	MKFG, CK, R			34	IRS52, IRAS49	IRAS 16246-2415			1
30B		32	51	Haro 1-11?								MC2169			
30C		33	53									MC2169			
31					642						IRS55, IRAS51?		ROC32		6
33	20	38	61		643	38	R				IRAS60?				7
34	13	40			266		CK, R, V853 Oph					IRAS 16257-2421			
35B									44						3
36							HD148562								
39														Src87	
42C												IRAS 16282-2427			8
43A												IRAS 16283-2423			9
43B									49			IRAS 16283-2423			3
44		44		Haro 1-16	268		CK, AJK					IRAS 16285-2421			
45D		48?													
45E		49													
45F		50													
47A		51			647		R		62						3

Notes:

1: Also detected at 1.3mm by André et al. (1990).
2: Additional near-IR measurements are in Chini (1981).
3: VSS only list optical polarization measurements for this star.
4: ROXs 14 (=S1) was extensively studied at 5 and 15 GHz by André et al. (1988) and André et al. (1991).
5: Also a 5 GHz radio source (Leous et al. 1990).
6: Sub-arcsecond binary (Simon et al. 1987, Zinnecker & Perrier 1988).
7: This star was noted as a non emission-line star by Struve & Rudkjøbing (1949). It now exhibits a strong P Cygni profile at Hα.
8: A double-lined spectroscopic binary with an orbital period of 35.95 days (Mathieu et al. 1989)
9: A single-lined spectroscopic binary with an orbital period of 89.1 days (Mathieu et al. 1989)

References:

Hα: *AS*=Merrill & Burwell (1950), *DoAr*=Dolidze & Arakelyan (1959), *Haro*=Haro (1949), *SR*=Struve & Rudkjøbing (1949), *WSB*=Wilking et al. (1987)
Optical: *AJK*=Appenzeller et al. (1983), *C*=Chini (1981), *CK*=Cohen & Kuhi (1979), *HBC*=Herbig & Bell (1988), *MKFG*=Montmerle et al. (1983), *R*=Rydgren (1980)
Infrared: *EL*=Elias (1978), *GSS*=Grasdalen et al. (1973), *IRAS sources*: Ichikawa & Nishida (1989), *MC*: quoted in WSB, *VSS*=Vrba et al. (1976), *WLY*=Wilking et al. (1989), *YLW*=Young et al. (1986)
Radio: *AMF*=André et al. (1987), *SFAM*=Stine et al. (1988)

© European Southern Observatory • Provided by the NASA Astrophysics Data System

1992A&AS...92..481B

TABLE 3. *Journal of spectroscopic observations.*

Date	Detector	Dispersion (Å/mm)	Spectral domain (Å)
07.24.83	IDS	172	4100-6800
07.25-28.83	EMI tube	39	3700-5000
08.12-14.83	EMI tube	39	3700-5000
"	"	59.5	5800-7700
04.08-12.84	IDS	114	3700-5500
"	"	114	3900-6000
"	"	116	5500-7700
07.13-18.84	IDS	116	5500-7500
"	"	224	3600-7300
"	"	224	3700-8000
06.10-21.85	IDS	116	5400-7700
05.14-19.86	IDS	116	5400-7700
		116	6400-8800

TABLE 5. *Night-to-night Hα equivalent width variations (Å).*

Date	6/10/85	6/11	6/12	6/13	6/15	6/16	6/17	6/19	6/20	6/21
ROXs 3	2.5	2.8	2.6	-	-	2.9	3.4	3.4	3.1	2.8
ROXs 21	4.8	4.9	5.3	6.5	3.5	6.0	5.5	4.1	6.2	5.5
ROXs 29	14.6	15.7	10.5	11.0	11.2	13.1	11.5	11.5	12.2	26.1
ROXs 44	51.1	33.1	38.0	33.0	31.6	33.8	37.1	52.3	50.5	53.7

TABLE 4. *Spectral types, equivalent widths of emission lines, and Li I λ6707.*

ROXs	Sp.T.	Hα (Å)	Hβ (Å)	CaII K (Å)	CaII H+Hε (Å)	Li I λ6707	Notes
2	K3/M0:	2.8				y	1
3	K3/M0	2.3/2.7 (v)	none	0.3	0.2	y	1
4	K2	2.5	none			y:	
5	K7	1.4				y	
6	K6	87/220 (v)	23/38 (v)	40.3	24.4	y	
7	K7	f:/1.5 (v?)	1.0:			y	
8	K0	-0.6	-0.8	0.5	0.15:	y	2
9A	M0	-1.0				n	
9B	K2	-0.5				?	
9C	K4	-1.0				n	
9D	G?	-3.8				n	
10A	K5	20	5.7			y	
10B	K0	5	none			y	
12	M0	f:/1.2 (v?)	none			y	
14	B4:	-3.5				n	3
16	G9:	19	2			y	4
20A	M5	3.0				n	
20B	M2	6.3	5.5			n	
21	K4/M2.5	4.5/8.8 (v)	1.5	2.9	3.0	y	1
29	K4/K6	10.5/13.8 (v)	3.7/4.8 (v)	5.6	5.9	y	1
30A	G?	-2.0	none			n	
30B	K4	22.2				y	
30C	K4	14.3				y	
31	K7	3.3	none			?	
33	G0:	21	0.9:			y:	5, 6
34	M2.5	30/48.3 (v)	18.5/26 (v)	14.8	31.2	y	
35A	K3	-1.0				n	
35B	G4	-2.0				n	
36	A2	-1.9				n	
38A	K2	-1.5				n	
38B	K?	-2.8				?	
39	K5	3.6/6.0 (v)				y	
40	K6	-1.2				n	
42A	<G5	-4.0	-2.0			?	7
42B	M0	1.7	none			y:	
42C	K6	f/1.6 (v?)	-1.9:			y	
43A	G0:	1.8/3.4 (v)	-3.4	-11.9	-10.3	y	6
43B	K5	0.8	-2.0:			y	
44	K3	60.5/76.1 (v)	13.7	16.8	11.4	y	
45A	F?	-8.1	-19.1		-4	n	
45B	K?	f:	none			n	
45C	K5	-1.0:	none			n	
45D	K0	-1.0:	none			n	
45E	K7	f	none			?	
45F	K7-M0	1.1	none			y	
47A	K2/K7-M0	9.2	0.4	0.3	0.3	y	1
47B	K3	-2.0:	none			?	

Notes:
1: The spectral type varies with wavelength, being earlier at shorter wavelengths (see text).
2: Hα was previously detected in emission by Dolidze & Arakelyan (1959).
3: The spectral type is earlier than G0. The FWHM and equivalent width of the Hα line suggest a spectral type B4.
4: The strong [OI] λ5577, 6300, and 6330 lines seen in the spectrogram may be due to sky contamination.
5: Strong P Cygni profile at Hα.
6: The spectral type is late F or early G
7: The spectral type is probably F or G.

© European Southern Observatory • Provided by the NASA Astrophysics Data System

1992A&AS...92..481B

TABLE 6. *UBVRI photometry, visual extinction, and stellar luminosity.*

ROXs	V	B-V	U-B	V-R_c	V-I_c	A_V	log $L/L_\odot$
2	15.4	2.2	1.3	1.5	3.1	5.9	0.7
3	13.2	1.5	1.3	1.0	2.0	0.6	-0.2
4	15.3	2.2	1.0	1.4	2.9	5.9	0.7
5	14.5			1.1		2.3	-0.2
6	12.8	1.5	-0.1	1.1	2.1	2.2	0.4
7	(16.9)			(1.5)	(3.3)	4.7	-0.2
8	13.9	2.2	1.2	1.5	3.0	6.6	1.5
9A				(1.3)		3.3	
9B				(1.1)		3.3	
9C				(0.9)		1.9	
9D				(0.8)		2.4:	
10A	14.2	1.9	1.4	1.2	2.4	3.3	0.2
10B	14.6	2.2	1.0	(1.5)		6.6	1.2
12	(15.4)	(2.0)		(1.1)		1.7	-0.7
14				(1.6)		10.3:	
16	(15.7)	(2.2:)		(1.4)		6.1:	0.6:
20A	(16.7:)			(1.5)		2.6	-0.3:
20B	(15.1)	(2.1:)		(1.1)		0.7	-0.8
20A+B	15.1	1.7	1.0				
21	13.4	1.5	1.2	1.0	2.3	0.6	-0.2
29	11.5	1.2	0.65	0.8	1.6	0.2	0.1
30A	(16.1)	(1.8:)		(1.1)	(2.4)	4.6:	-0.2:
30B	15.4			1.3		4.1	0
30C	15.0			1.2		3.6	0
31	(16.8)	(2.3:)		(1.4)	(3.3)	4.3	-0.3
33	14.0	2.0	1.2	1.4	2.7	6.5:	1.3:
34	13.3	1.1	-0.35	0.95	2.4	0	-0.2
35A	(12.6:)			(0.9)		1.7	0.1:
35B				(0.4)		0	
36	8.2			(0.1)		0.4	1.2
38A				(1.0)		3.0	
38B				(1.1)		2.4:	
39	(13.0)			(1.1)		2.4	0.3
40				(1.0)		1.6	
42A	(15.2)	(1.4:)		(0.9)	(1.9:)	3.1:	-0.5:
42B	(15.0)	(2.2:)		(1.2)	(2.7:)	2.5	-0.2
42C	(12.5)	(1.7)		(1.0)	(2.1)	1.9	0.4
43A	(11.4)	(1.3)		(0.8)	(1.6)	2.3:	0.7:
43B	(12.3)	(2.1)		(0.9)	(1.9)	1.3	0.2
44	12.6	1.35	0.55	0.9	1.8	2.1	0.3
45A	(13.7)	(1.1)		(0.8)	(1.6:)	2.8:	0.0:
45B	(17.4)			(1.3)	(2.8:)	4.4:	-0.6:
45C	(16.0)	(2.2:)		(1.3)	(2.7:)	3.9	-0.25
45D	(15.1)	(1.7)		(1.0)	(2.0:)	3.3	-0.3
45E	(13.5)	(1.4)		(0.8)	(1.5:)	0.1	-0.7
45F	(13.8)	(1.5)		(0.9)	(1.7:)	0.3	-0.7
47A	13.6	1.7	1.1	1.2	2.5	2.3	0.2
47B	(12.3)	(1.25)		(0.6)		0.2	-0.3

© European Southern Observatory • Provided by the NASA Astrophysics Data System

1992A&AS...92..481B

TABLE 7. *UBVRI photometry: Individual measurements.*

ROXs	Date	V	B-V	U-B	V-R_c	V-I_c
2	8/4/83	15.53	2.37		1.49	3.10
	8/8/83	15.36	1.79	1.32		
	8/8/83	15.36	2.56			
4	8/4/83	15.32	2.26	0.12	1.44	2.91
	8/8/83	15.31	2.13	2.37		
	8/8/83	15.28	2.18			
	8/8/83	15.31	2.04	0.62		
10A	8/4/83	14.25	1.90	0.86	1.20	2.41
	8/7/83	14.09	1.84	0.90		
	8/7/83	14.11	1.90	1.88		
	8/8/83	14.19	1.86	1.95		
	8/8/83	14.20	1.88	1.51		
10B	8/8/83	14.60	2.33	0.90		
	8/8/83	14.57	2.13	1.16		
20 A+B	8/8/83	15.10	1.71	1.11		
	8/8/83	15.09	1.77	0.92		
33	8/4/83	14.05	1.97	1.15	1.39	2.72
	8/7/83	14.0	2.10	0.91		
	8/8/83	14.04	1.96	1.31		
	8/8/83	14.07	2.01	1.32		

Note: UBVRI photometry for ROXs 3, 6, 8, 21, 29, 34, 44, and 47A has been published in Bouvier et al. (1988).

TABLE 8. *JHKLM photometry.*

Star	J.D. 244	J	H	K	L	M
ROXs 6	5719.65	9.2	8.3	7.4	6.4	6.5
	5721.61	9.5	8.3	7.9	7.4	6.3
	5722.63	9.2	8.0	8.1	8.6	7.8
ROXs 8	5719.62	8.3	6.9	6.5	5.7	6.0
	5721.58	8.3	6.9	6.3	5.8	5.2
	5722.57	8.2	6.8	6.2	5.8	5.3
ROXs 29	5719.65	8.5	7.7	7.3	6.4	6.6
	5721.64	8.5	7.7	7.2	6.4	6.0
	5722.61	8.5	7.7	7.2	6.5	6.0
ROXs 47A	5722.59	9.1	8.2	7.9	7.4	7.5

© European Southern Observatory • Provided by the NASA Astrophysics Data System

1992A&AS...92..481B

FIGURE 1. Finding charts for the optical counterpart candidates of ρ Ophiuchus X-ray sources. North is at the top, and east is to the left.

© European Southern Observatory • Provided by the NASA Astrophysics Data System

1992A&AS...92..481B

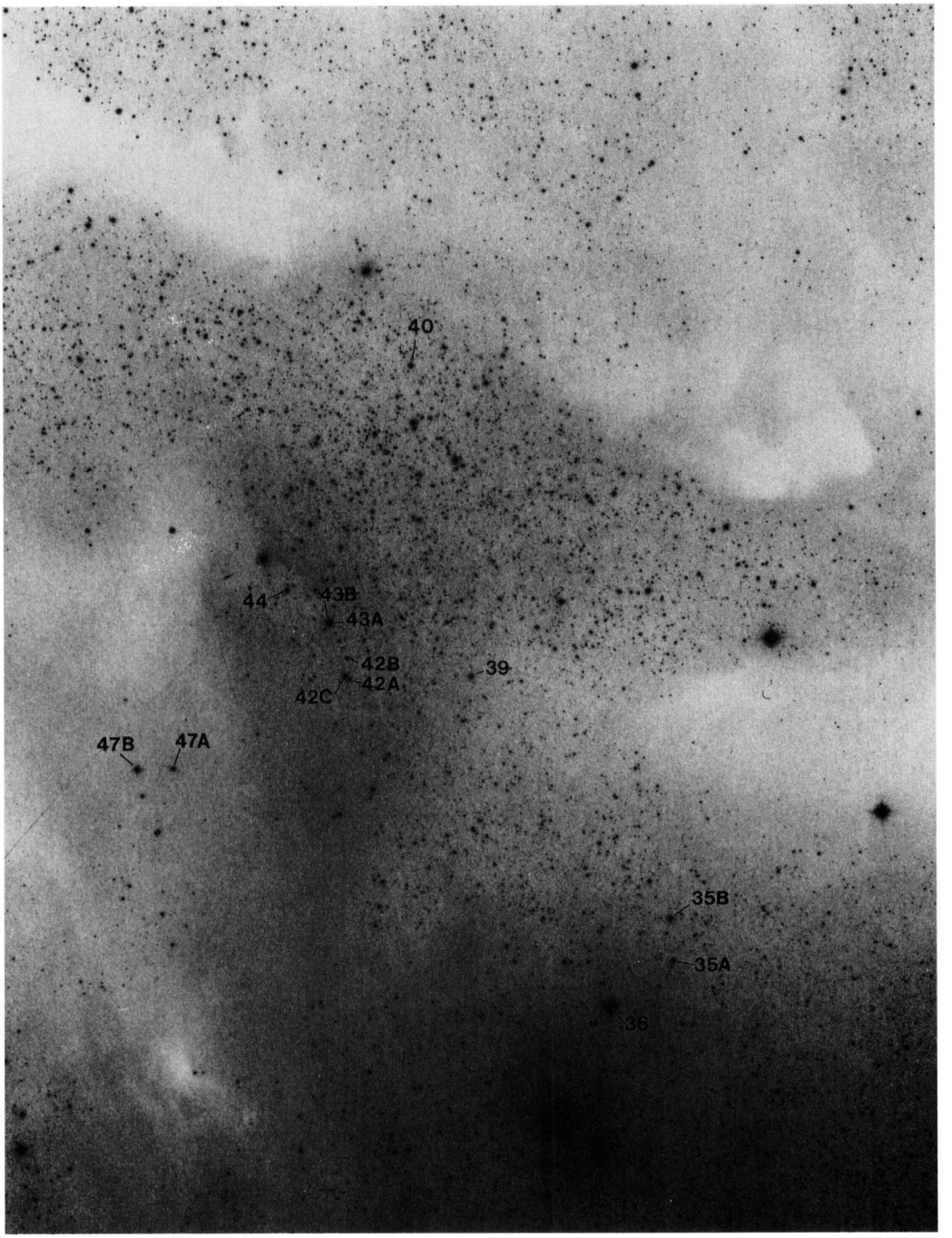

FIGURE 1. (*continued*)

© European Southern Observatory • Provided by the NASA Astrophysics Data System

1992A&AS...92..481B

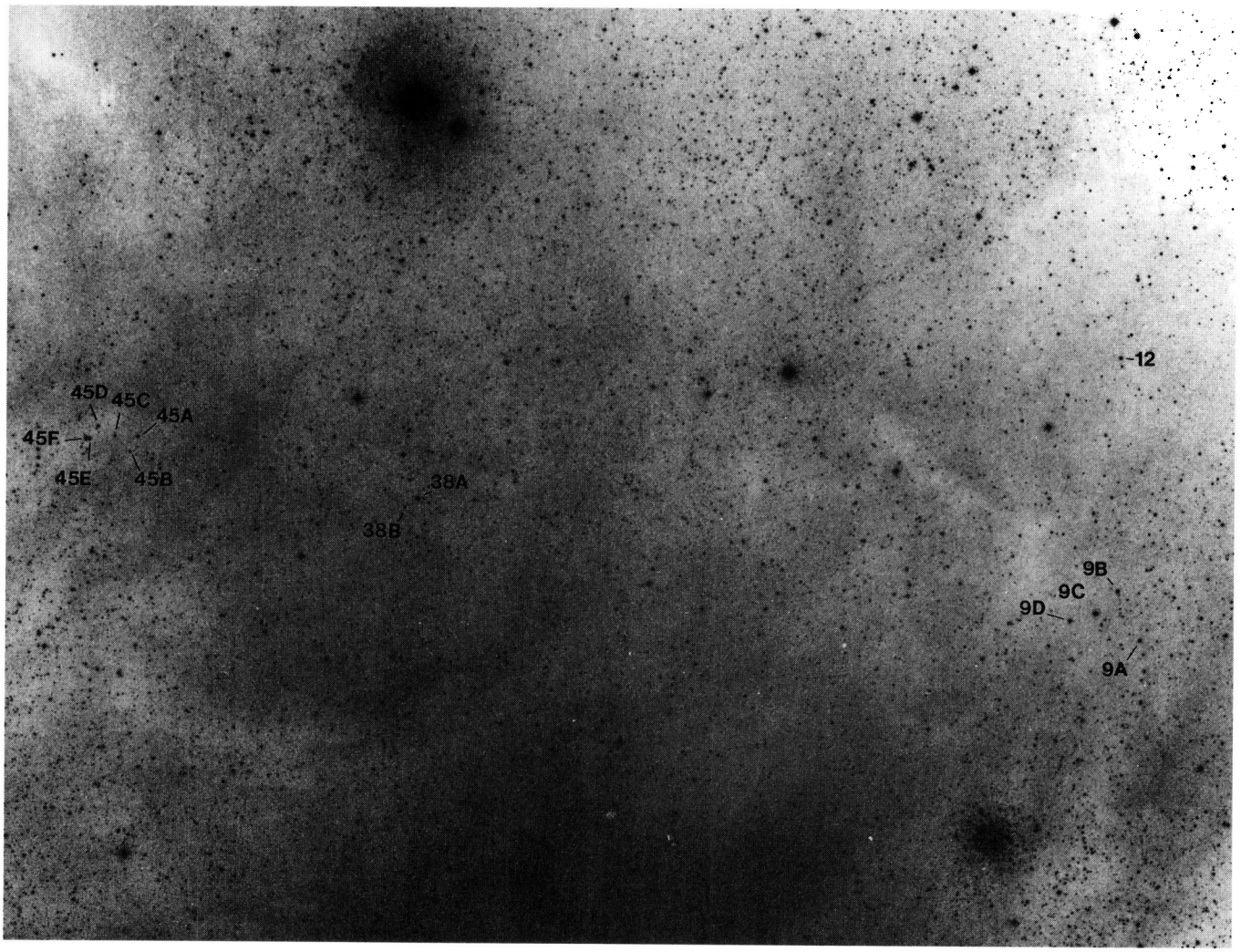

FIGURE 1. (*continued*)

© European Southern Observatory • Provided by the NASA Astrophysics Data System

1992A&AS...92..481B

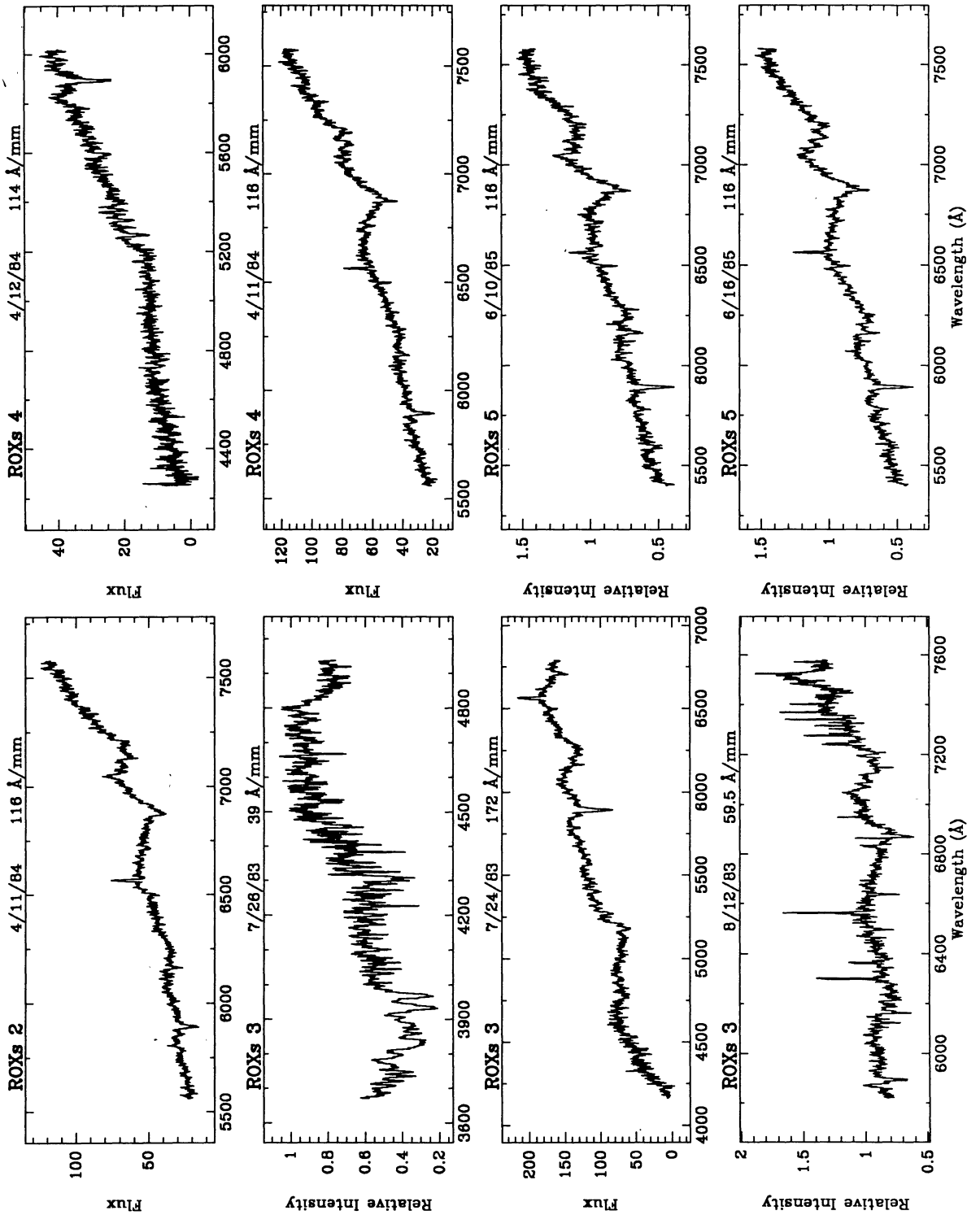

FIGURE 2. Low- and medium-resolution spectrograms of the ROX optical counterpart candidates. The spectrograms are ordered by increasing ROX source number. The date of observation and the spectral dispersion are given above each panel. The ordinate scale for flux-calibrated spectrograms is in units of 10^{-16} erg cm^{-2} Å^{-1}. Otherwise, relative intensity are shown. The spectrograms of strong emission-line stars are plotted on two intensity scales. The ordinate scale refers to the higher plot. The scale of the lower plot is reduced by a factor given in the lower right corner of the panel. Note that image tube spectrograms may be strongly affected by sky emission-lines.

© European Southern Observatory • Provided by the NASA Astrophysics Data System

1992A&AS...92..481B

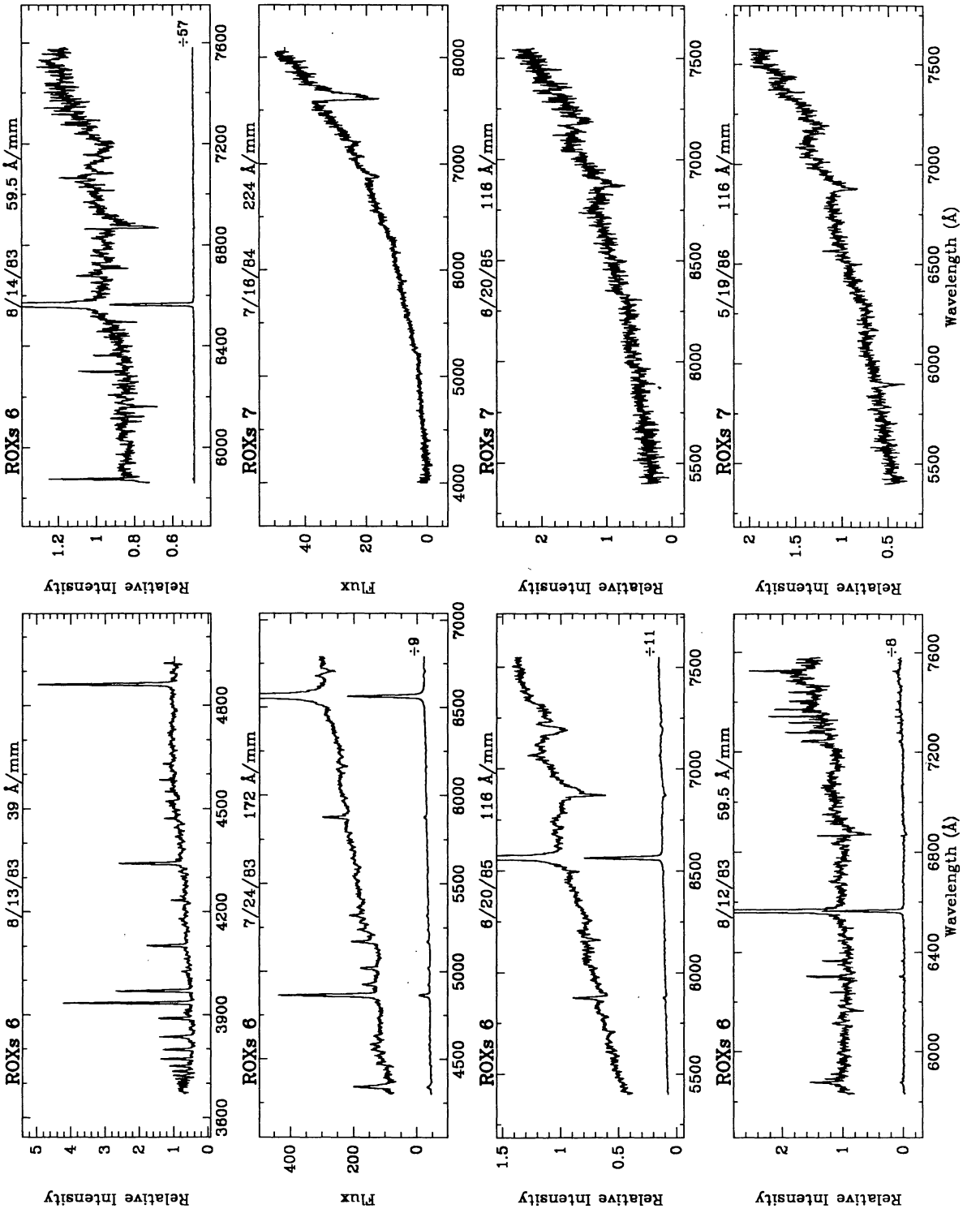

FIGURE 2. (*continued*)

© European Southern Observatory • Provided by the NASA Astrophysics Data System

1992A&AS...92..481B

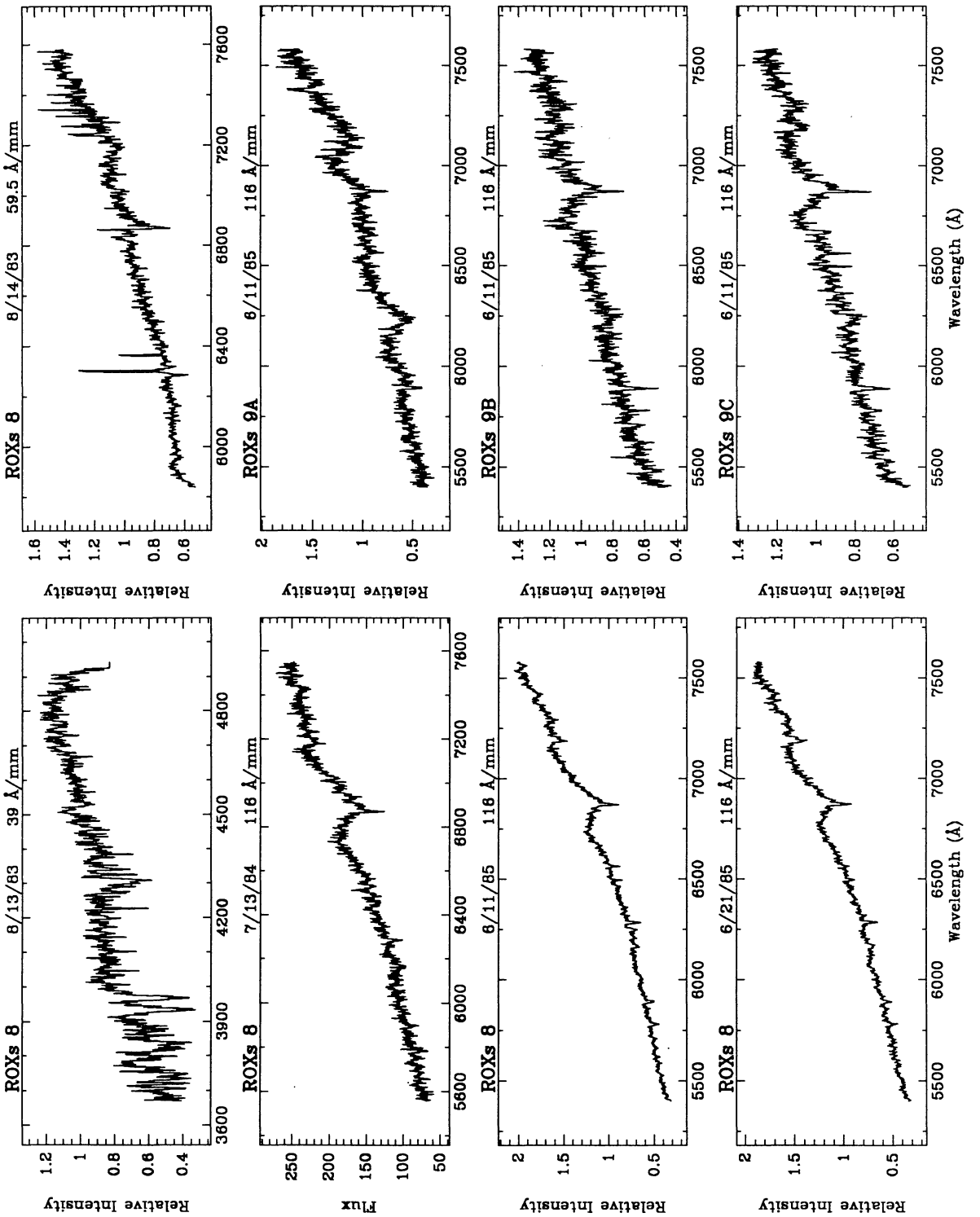

FIGURE 2. (*continued*)

© European Southern Observatory • Provided by the NASA Astrophysics Data System

1992A&AS...92..481B

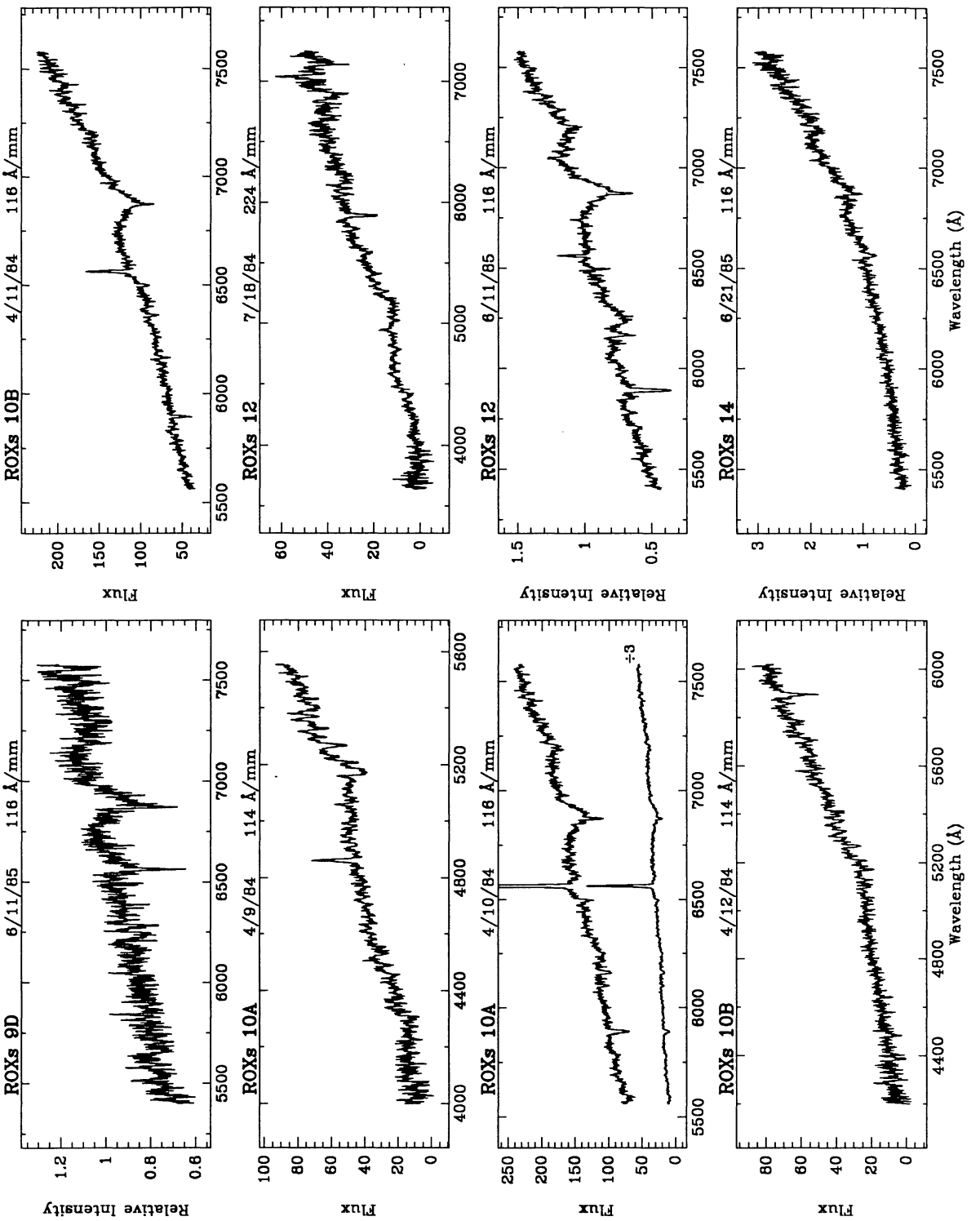

FIGURE 2. (*continued*)

© European Southern Observatory • Provided by the NASA Astrophysics Data System

1992A&AS...92..481B

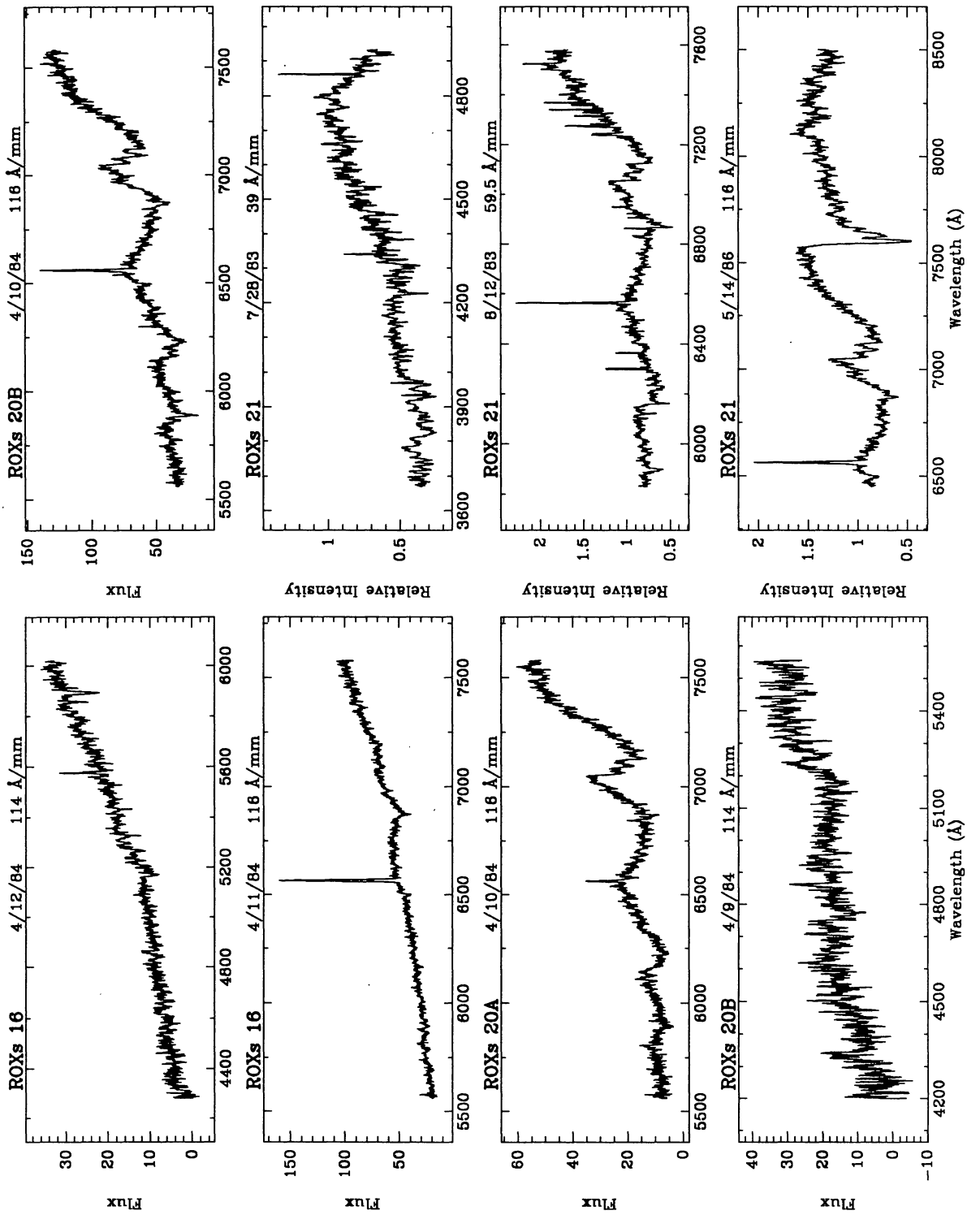

FIGURE 2. (*continued*)

© European Southern Observatory • Provided by the NASA Astrophysics Data System

1992A&AS...92..481B

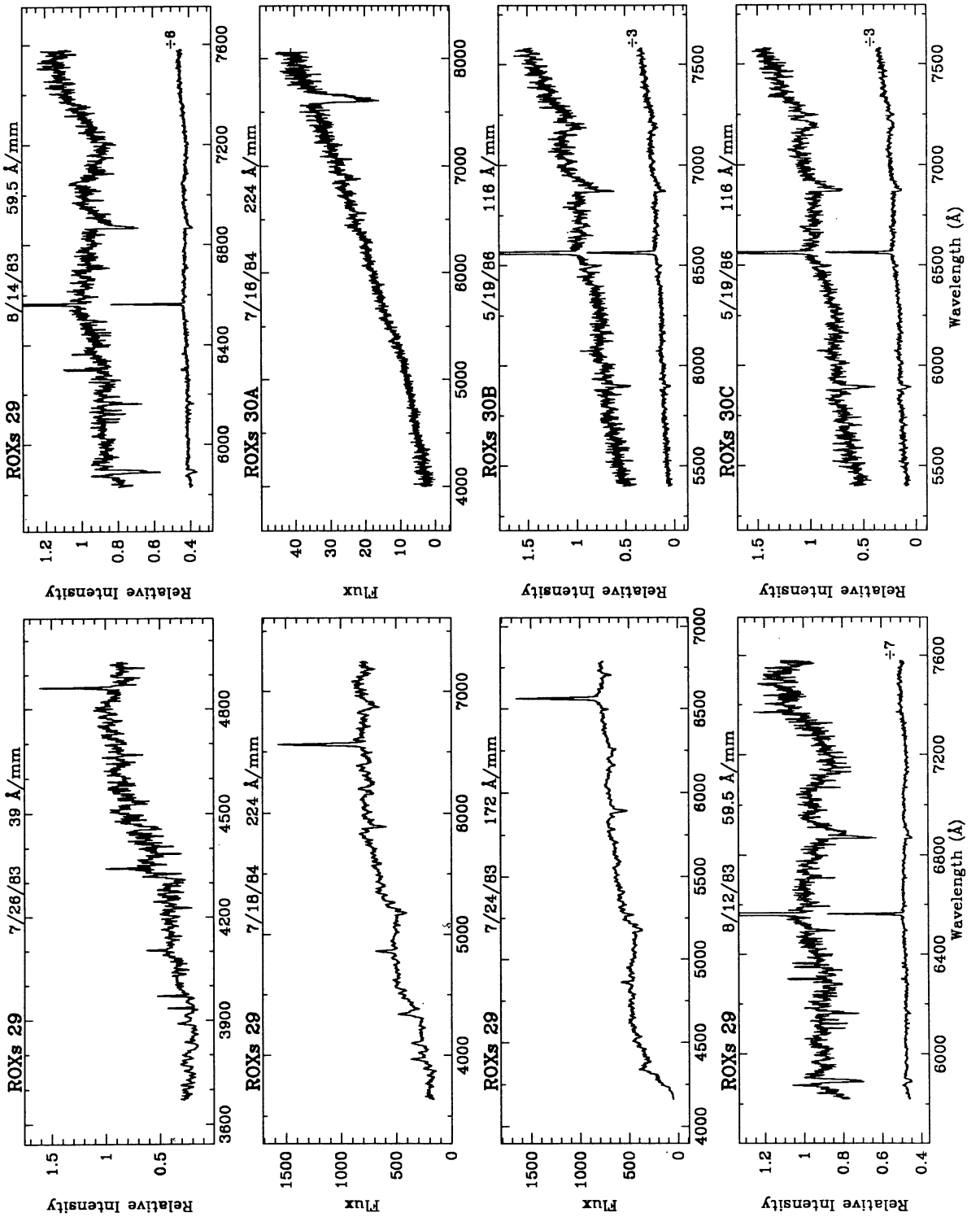

FIGURE 2. (*continued*)

© European Southern Observatory • Provided by the NASA Astrophysics Data System

1992A&AS...92..481B

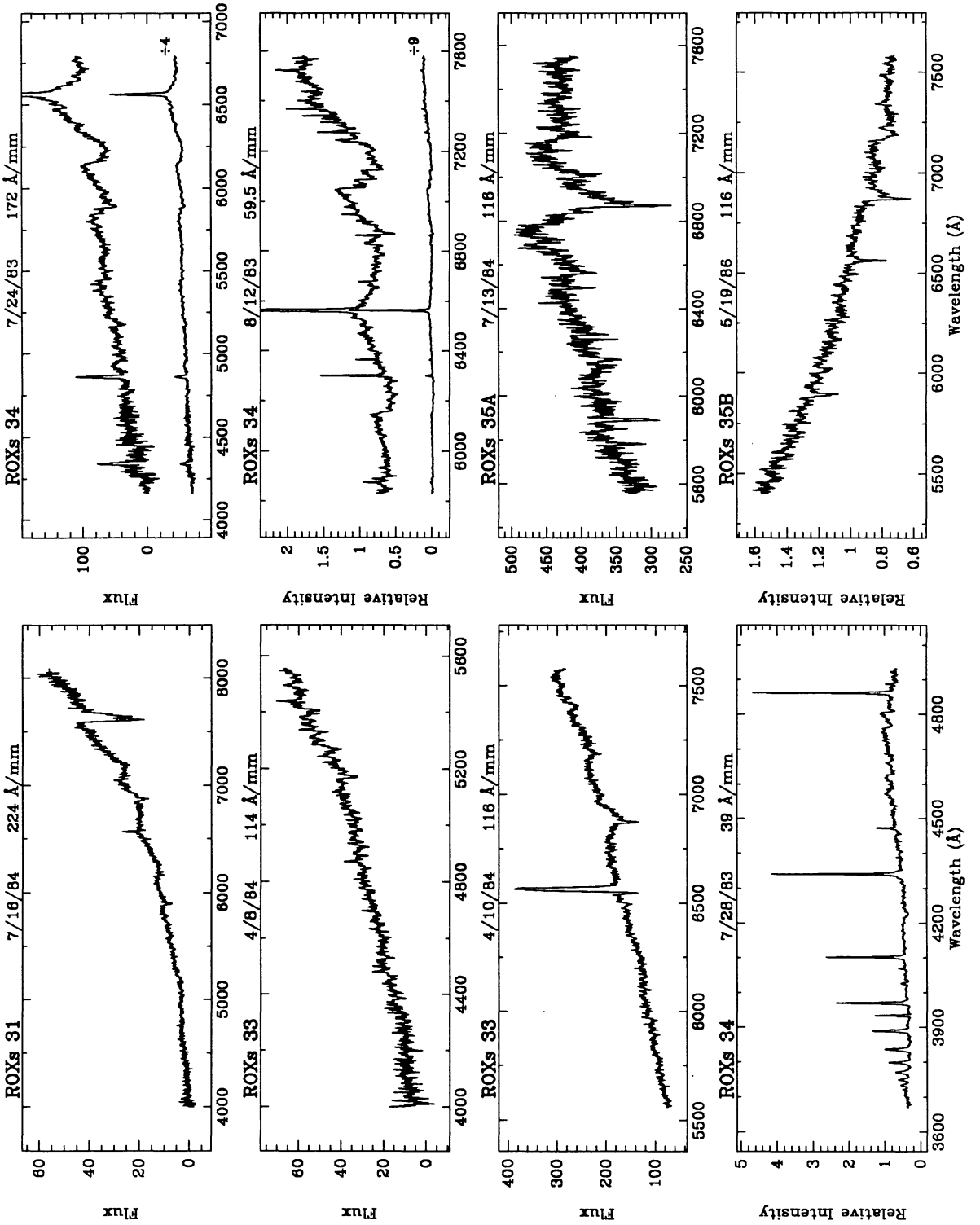

FIGURE 2. (*continued*)

© European Southern Observatory • Provided by the NASA Astrophysics Data System

1992A&AS...92..481B

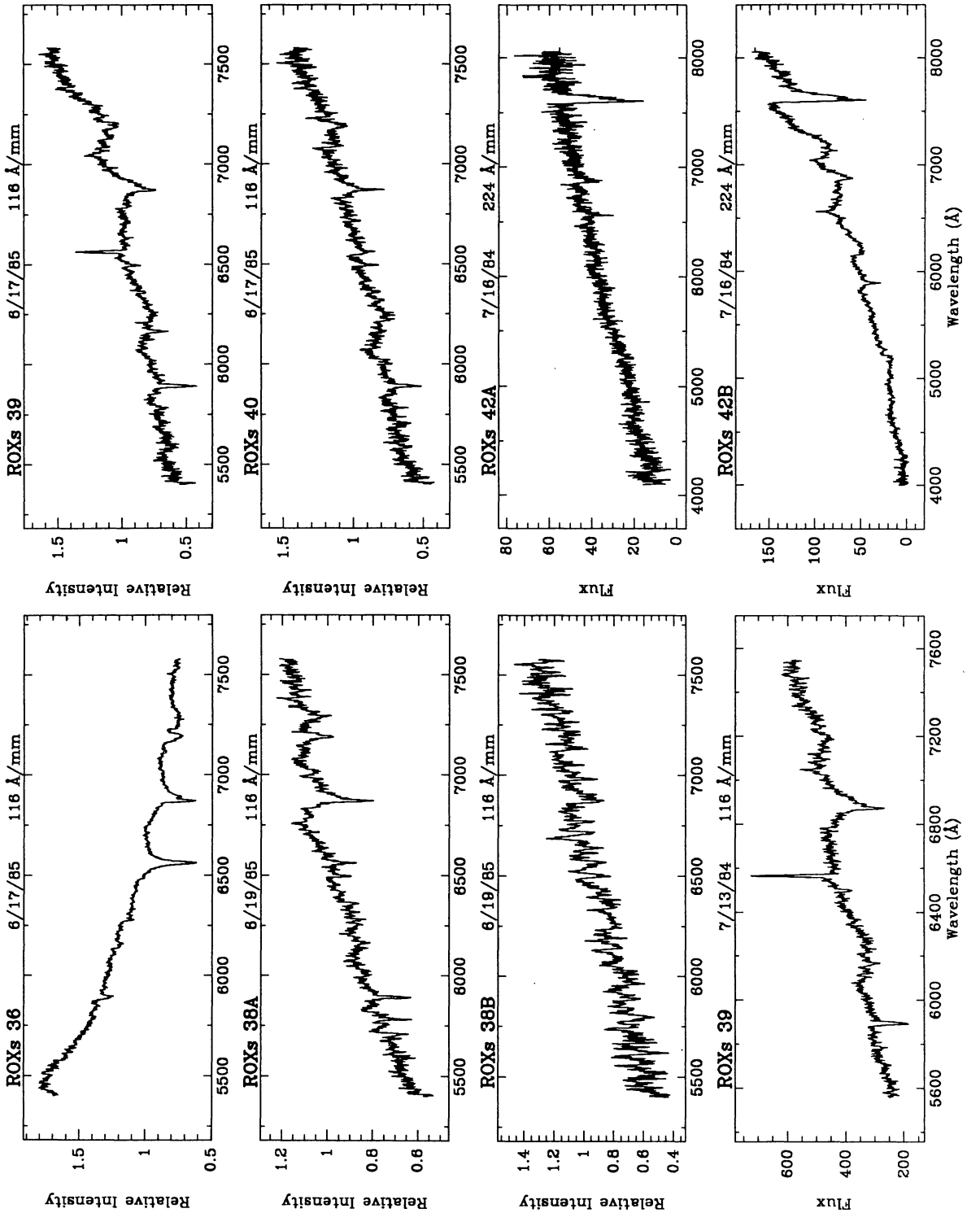

FIGURE 2. (*continued*)

© European Southern Observatory • Provided by the NASA Astrophysics Data System

1992A&AS...92..481B

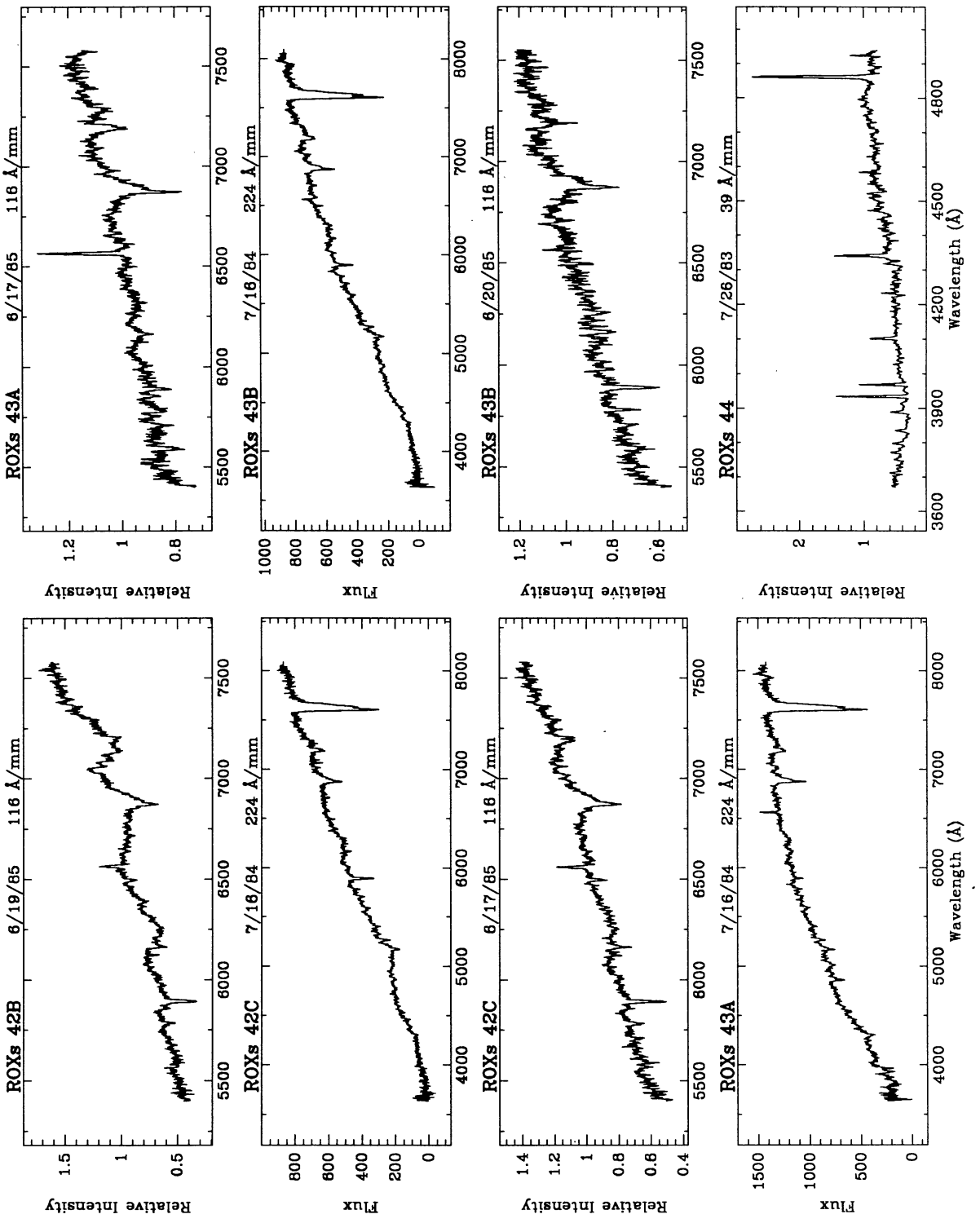

FIGURE 2. (*continued*)

© European Southern Observatory • Provided by the NASA Astrophysics Data System

1992A&AS...92..481B

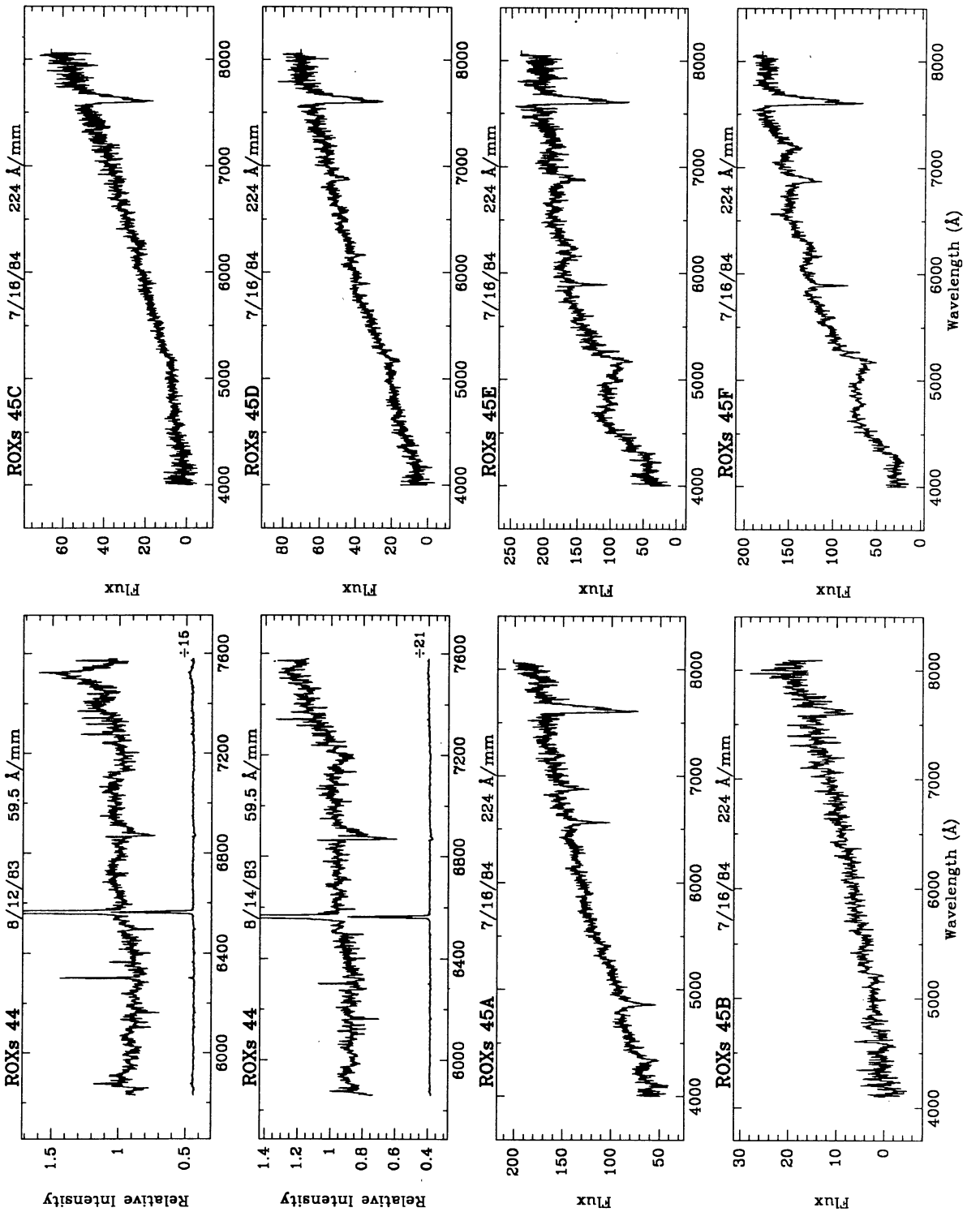

FIGURE 2. (*continued*)

© European Southern Observatory • Provided by the NASA Astrophysics Data System

1992A&AS...92..481B

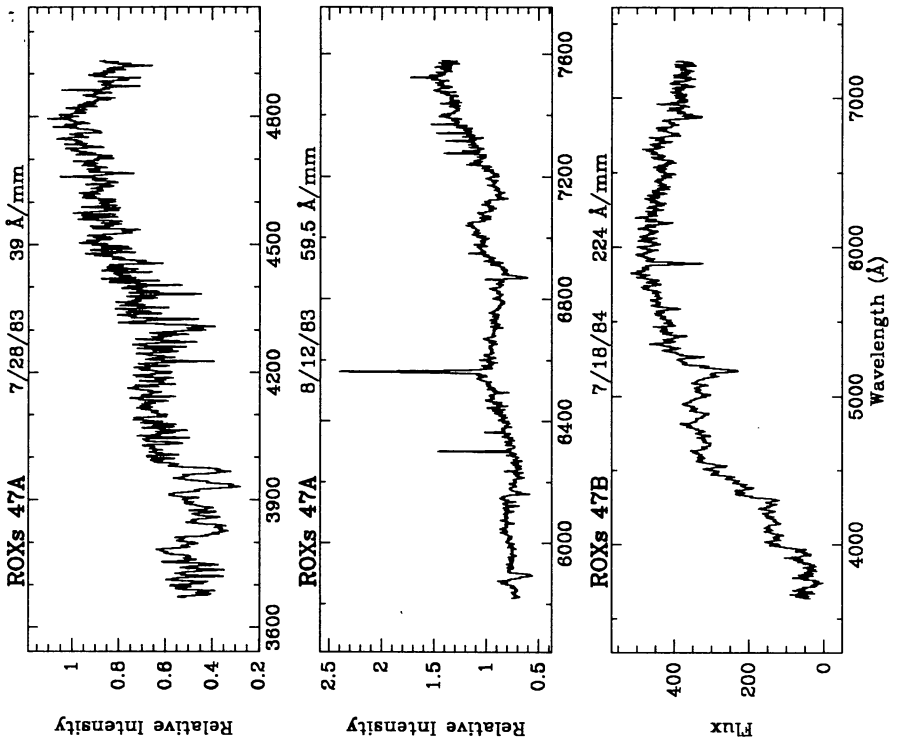

FIGURE 2. (*continued*)

© European Southern Observatory • Provided by the NASA Astrophysics Data System

1992A&AS...92..481B

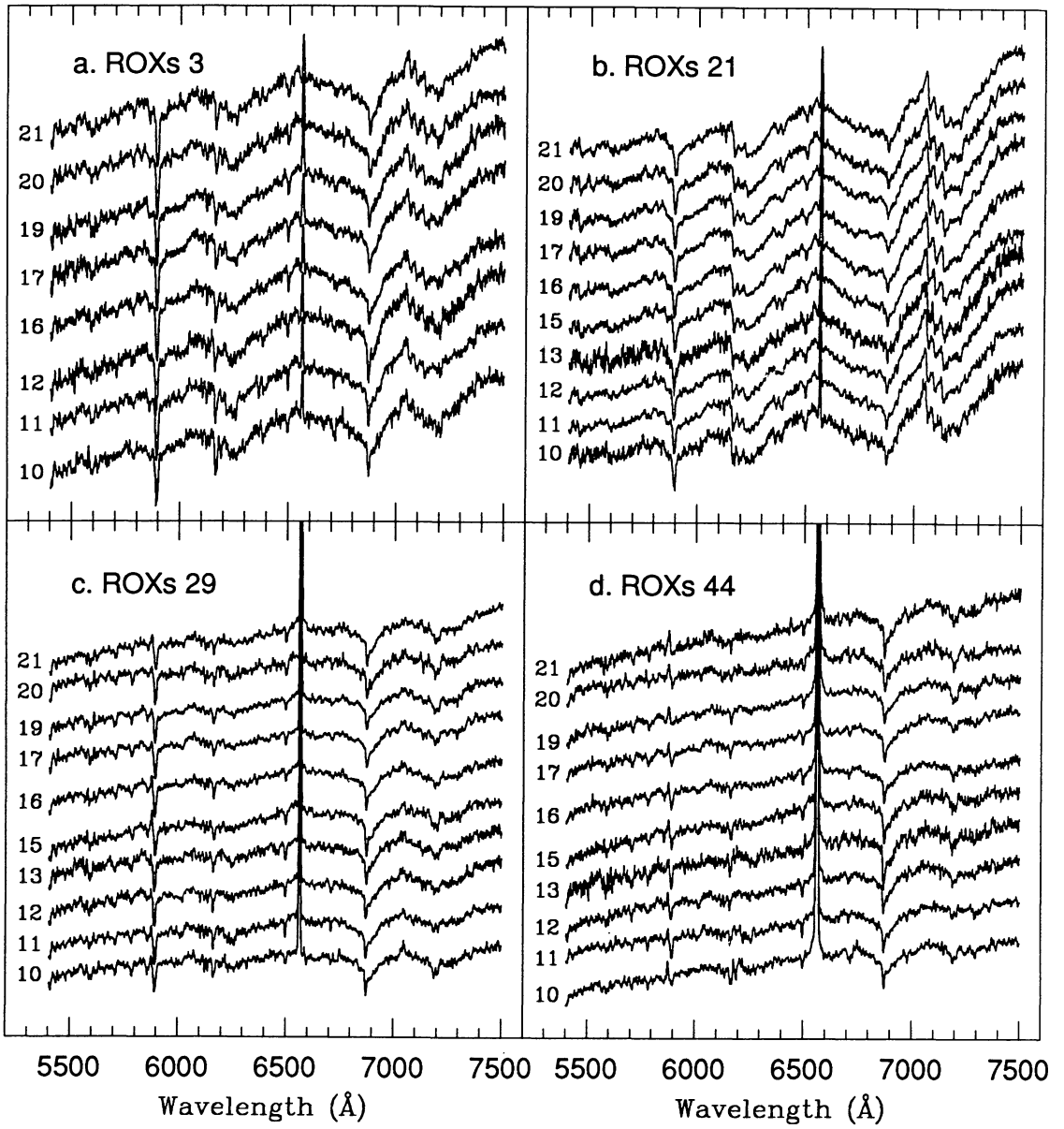

FIGURE 3. Low-resolution spectrograms of a) ROXs 3, b) ROXs 21, c) ROXs 29, and d) ROXs 44 obtained on a night-to-night basis between June 10 and June 21, 1985. An arbitrary offset has been applied to the spectrograms in each panel to allow direct comparison.

© European Southern Observatory • Provided by the NASA Astrophysics Data System

1992A&AS...92..481B

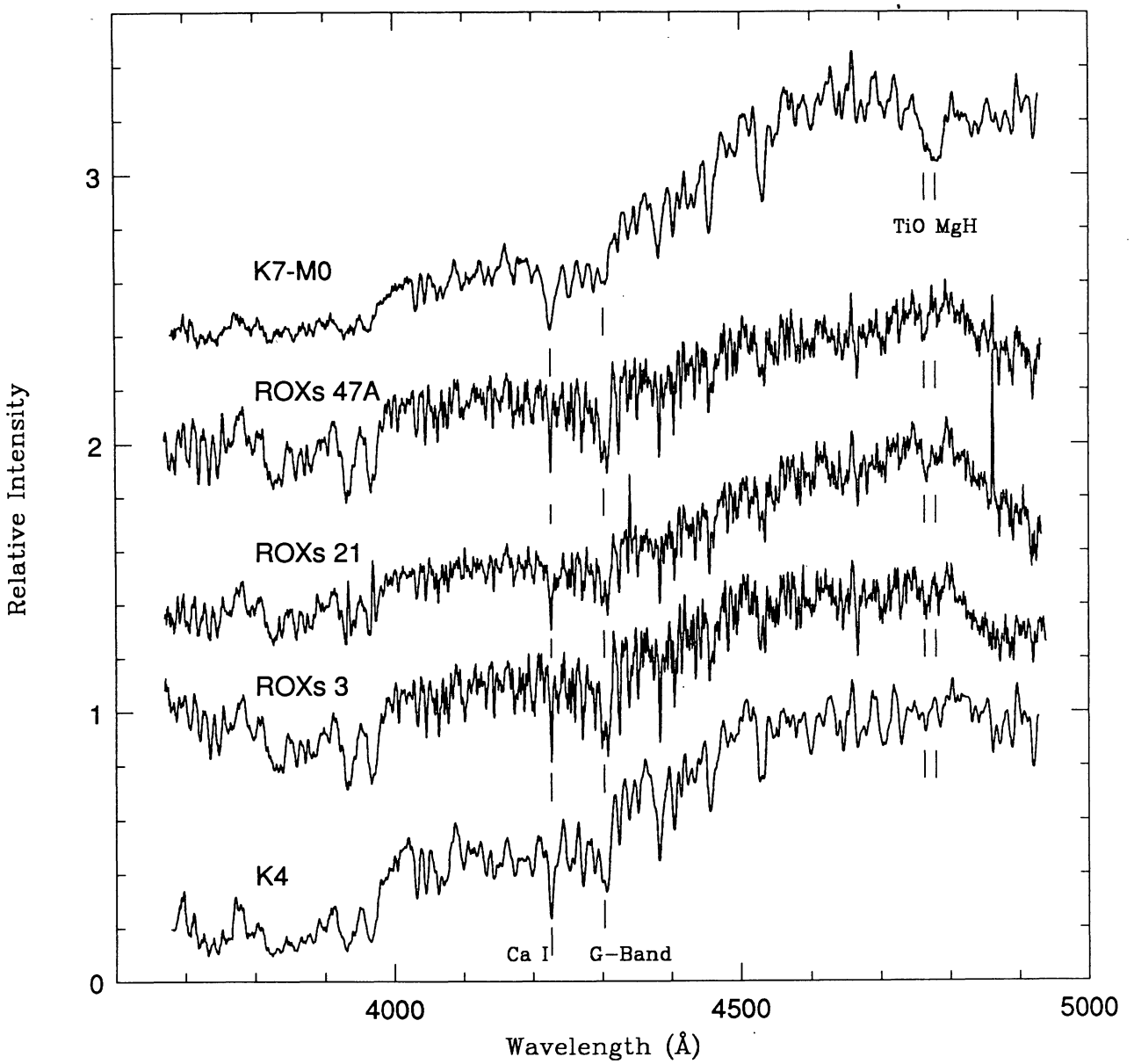

FIGURE 4. a)

FIGURE 4. a) Medium-resolution spectrograms of ROXs 3, 21, and 47 A in the 3700-4950 Å spectral region. The spectrograms of two standard stars, with a spectral type K4 and K7-M0, respectively, are shown for comparison. b) Same as a) for the 5800-7200 Å spectral region. The late-type standard star has a spectral type M0. The Hα line in the red spectrograms of ROXs 21 and 47A has been truncated for clarity. An arbitrary offset has been applied to the spectrograms in each panel to allow direct comparison. The spectrograms of the ROX stars were obtained with a higher spectral resolution than those of the standard stars, which results in a noisy appearance. In the blue range, the ROX stars have a photospheric spectrum similar or slightly earlier than that of the K4 template, while in the red range, deep TiO bands indicate a spectral type M0 or slightly later.

© European Southern Observatory • Provided by the NASA Astrophysics Data System

1992A&AS...92..481B

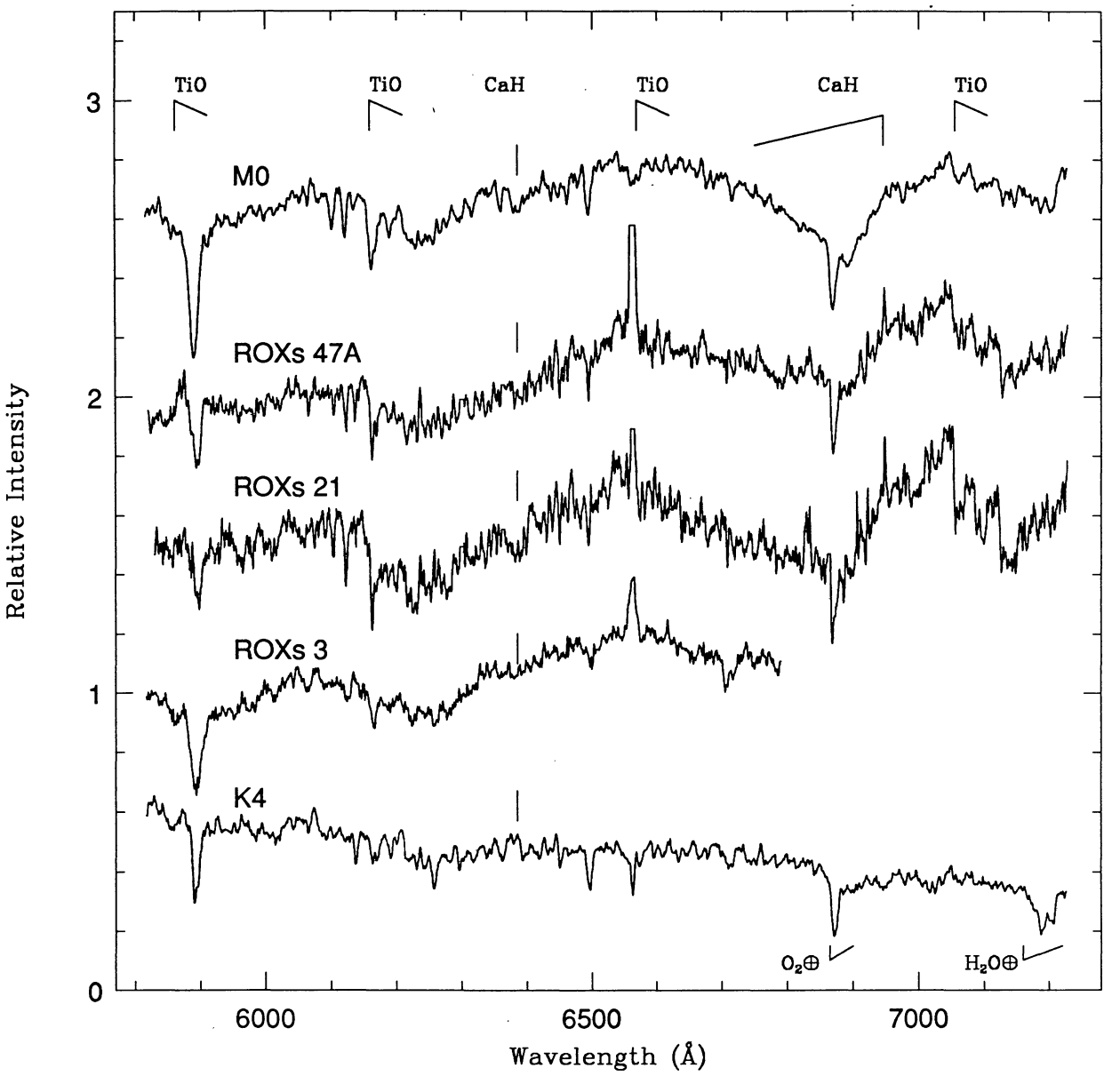

FIGURE 4. b)

© European Southern Observatory • Provided by the NASA Astrophysics Data System

1992A&AS...92..481B

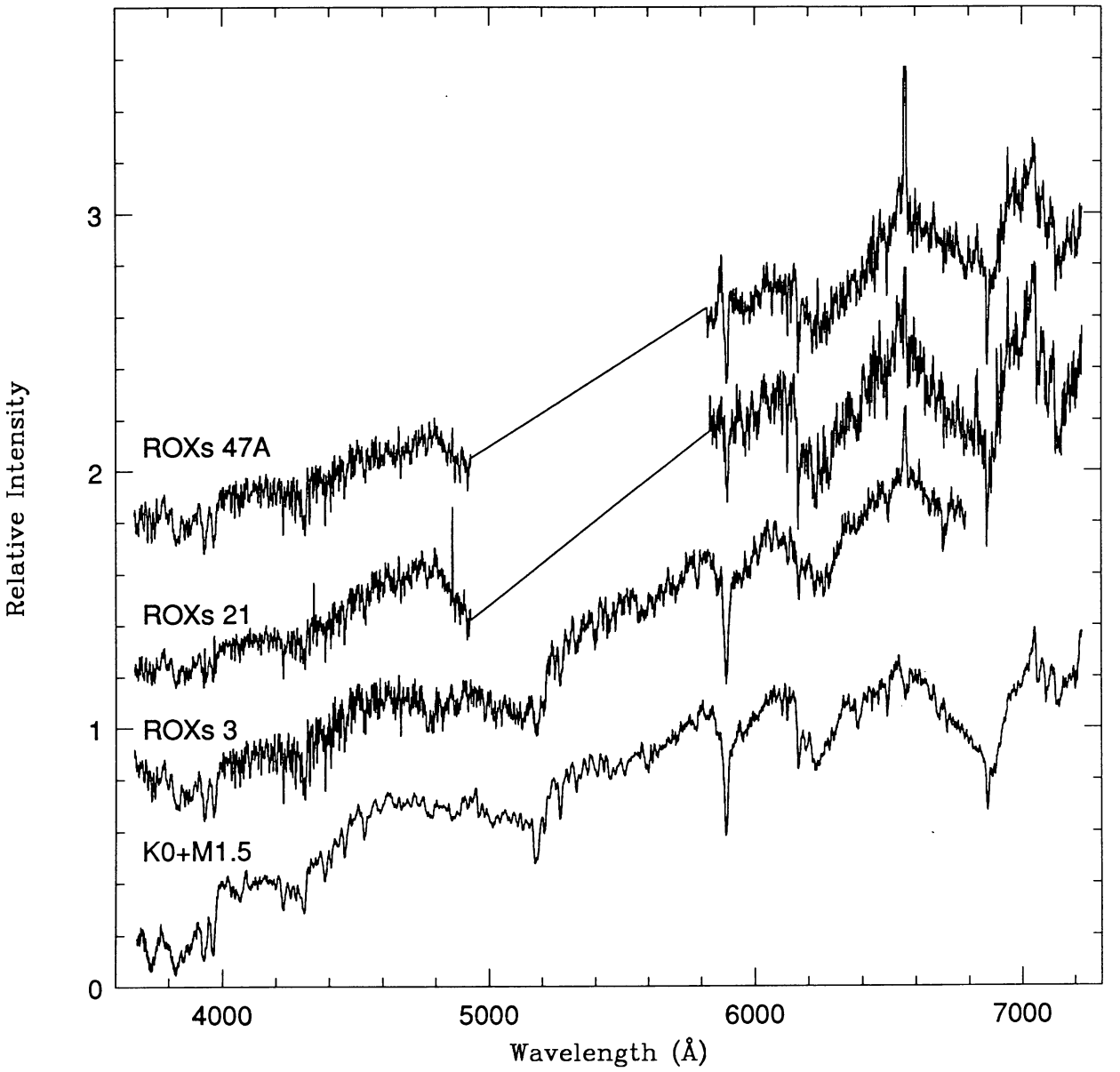

FIGURE 5. Composite spectra of ROXs 3, 21, and 47A over the 3700-7200 Å region. The lower spectrum was obtained by summing the spectrograms of two standard stars with a spectral type K0 and M1.5, respectively, after normalization to the same flux at 5500 Å (see text). An arbitrary offset has been applied to the spectrograms to allow direct comparison. The synthetic spectrum approximates the spectral type variation as a function of wavelength observed in the 3 ROX stars.

© European Southern Observatory • Provided by the NASA Astrophysics Data System

1992A&AS...92..481B

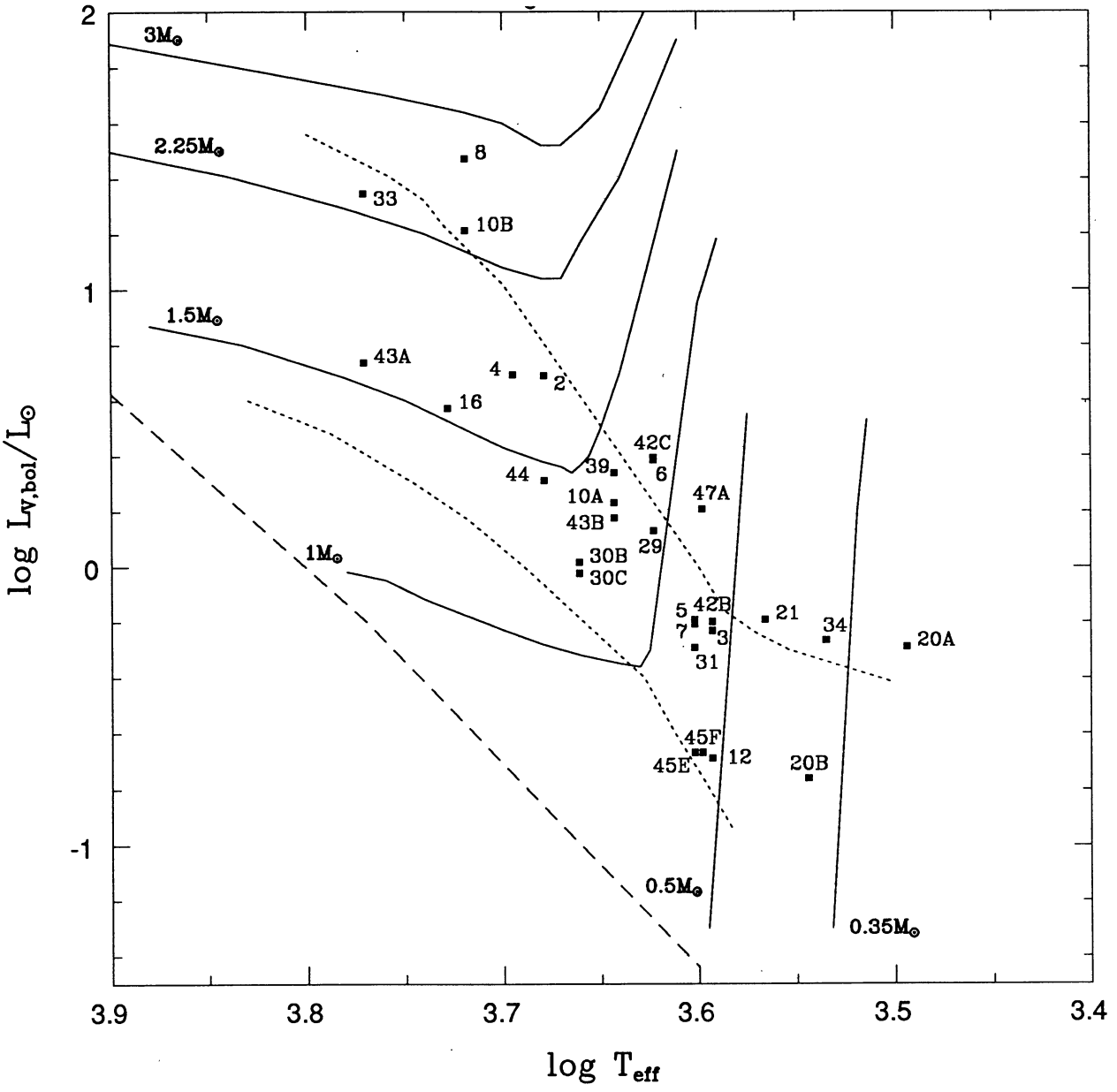

FIGURE 6. Distribution of the identified X-ray emitting cloud members in the HR diagram. The stars are labelled with their respective ROXs number. The spectral type deduced from the red spectral region has been adopted for the ROX stars which exhibit spectral type variations as a function of wavelength. Solid lines are theoretical pre-main sequence evolutionary tracks for stars with a mass between 0.35 and 3 $M_{\odot}$. The theoretical zero-age main sequence locus is shown as a dashed line. The upper and lower dotted lines are theoretical isochrones corresponding to an age of 10^6 and 10^7 yr, respectively. The location of the X-ray emitting cloud members in the HR diagram is similar to that of *bona fide* T Tauri stars of the Taurus-Auriga association.

© European Southern Observatory • Provided by the NASA Astrophysics Data System

1992A&AS...92..481B

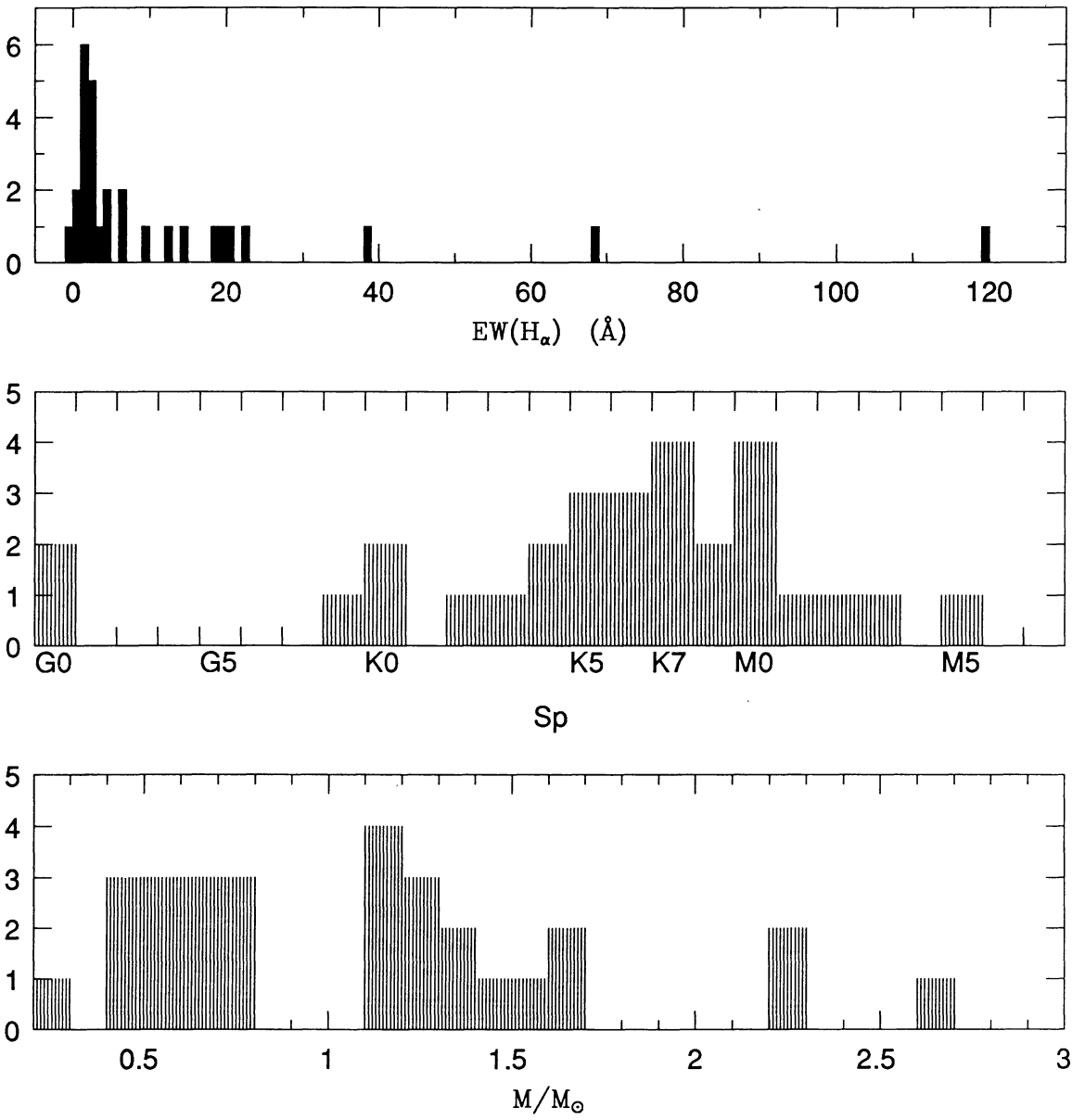

FIGURE 7. Histograms of Hα equivalent width, spectral type, and stellar mass for the ρ Ophiuchus pre-main sequence X-ray sources.

© European Southern Observatory • Provided by the NASA Astrophysics Data System